Network and receptor architectures shape brain morphometry in addiction

Foivos Georgiadis[1*], Beatrice A. Milano[2,3*], Sara Larivière[4], Kent E. Hutchinson[5], Vince Calhoun[6,7], Chiang-Shan Ray Li[8], Reza Momenan[9], Rajita Sinha[10], Dick Veltman[11], Ruth van Holst[11], Anneke Goudriaan[11], Maartje Luijten[12], Martine Groefsema[12], Henrik Walter[13], Tristram Lett[13], Reinout Wiers[14], Lianne Schmaal[15], Julianne Flanagan[16], Bernice Porjesz[17], Jonathan Ipser[18], Justin Boehmer[13], Nicola Canessa[19], Ramiro Salas[20], Edythe London[21], Martin Paulus[22], Dan Stein[18], Samantha Brooks[23], Liesbeth Reneman[24], Anouk Schrantee[24], Francesca Filbey[25], Rob Hester[26], Murat Yücel[27], Valentina Lorenzetti[28], Nadia Solowij[29], Rocío Martín-Santos[30], Albert Batalla[31], Janna Cousijn[32], Edith Pomarol-Clotet[33], Eduardo A. Garza-Villarreal[34], Marco Leyton[35], Elliot Stein[36], Cleo L. Crunelle[37], Anne M. Kaag[38], Antonio Verdejo-Garcia[39], John J. Foxe[40], Kathleen T. Brady[16], Aimee McRae-Clark[16], Alain Dagher[35], Amelie Haugg[1], Marc Walter[41], André Schmidt[42], Anne Lingford-Hughes[43], Louise M. Paterson[43], Angelica M. Morales[44], Dara G. Ghahremani[45], Chuan Fan[46], Etna J. E. Engeli[1], Marcus Herdener[1], Boris B. Quednow[1,47], Erich Seifritz[1,47], Philipp Homan[1], Marco De Pieri[2], Silke Bachmann[2,48], Daniele Zullino[49,50], Justine Y. Hansen[51], Bratislav Misic[51], Sophia I. Thomopoulos[52], Paul M. Thompson[52], Devarshi Pancholi[53], Anthony Juliano[53], Hugh Garavan[53], Sofie L. Valk[54,55,56,57], Boris C. Bernhardt[51], Matthias Kirschner[1,2,50], *the ENIGMA Addiction Working Group*

[*]Equal contributions: Foivos Georgiadis, Beatrice A. Milano

Corresponding authors: foivos.georgiadis@bli.uzh.ch; beatrice.milano@unige.ch; matthias.kirschner@unige.ch

Affiliations

[1]Department of Adult Psychiatry and Psychotherapy, University Hospital of Psychiatry Zurich (PUK), University of Zurich, Zurich, Switzerland

[2]Division of Adult Psychiatry, Department of Psychiatry, University Hospitals of Geneva, Geneva, Switzerland

[3]Institute of Life Sciences, Sant'Anna School of Advanced Studies, Pisa, Italy

[4]Department of Medical Imaging and Radiation Sciences, Université de Sherbrooke, Sherbrooke, QC, Canada

[5]Department of Psychiatry, University of Colorado Anschutz Medical Campus, Aurora, CO, USA

[6]Department of Psychology, School of Psychology, Georgia Institute of Technology, Atlanta, GA, USA

[7]Department of Psychiatry and Behavioral Sciences, Emory University School of Medicine, Atlanta, GA, USA

[8]Department of Psychiatry and Department of Neuroscience, Yale University School of Medicine, New Haven, CT 06510, USA

[9]Clinical NeuroImaging Research Core, National Institute on Alcohol Abuse and Alcoholism (NIAAA), National Institutes of Health (NIH), Bethesda, MD, USA

[10]Department of Psychiatry, Yale University School of Medicine, Yale Interdisciplinary Stress Center, New Haven, CT, USA

[11]Department of Psychiatry, Amsterdam UMC, University of Amsterdam, Amsterdam, The Netherlands

[12]Behavioural Science Institute, Radboud University Nijmegen, Nijmegen, The Netherlands

[13]Department of Psychiatry and Psychotherapy, Charité – Universitätsmedizin Berlin, Berlin, Germany

[14]Department of Psychology, University of Amsterdam, Amsterdam, The Netherlands

[15]Centre for Youth Mental Health, University of Melbourne, Melbourne, VIC, Australia

[16]Department of Psychiatry and Behavioral Sciences, Medical University of South Carolina, Charleston, SC, USA

[17]Department of Psychiatry, SUNY Downstate Health Sciences University, Brooklyn, NY, USA

[18]Department of Psychiatry and Mental Health, University of Cape Town, Cape Town, South Africa

[19]IUSS Cognitive Neuroscience (ICoN) Center, Scuola Universitaria Superiore IUSS, 27100, Pavia, Italy; Istituti Clinici Scientifici Maugeri IRCCS, Cognitive Neuroscience Laboratory of Pavia Institute, 27100, Pavia, Italy

[20]Department of Psychiatry and Behavioral Sciences, Baylor College of Medicine, Houston, TX, USA

[21]Department of Psychiatry, David Geffen School of Medicine, University of California Los Angeles, Los Angeles, CA, USA

[22]Laureate Institute for Brain Research, Tulsa, OK, USA

[23]School of Psychology, Faculty of Health, Liverpool John Moores University, UK

[24]Department of Radiology and Nuclear Medicine, Amsterdam UMC, University of Amsterdam, Amsterdam, The Netherlands

[25]Department of Psychology, University of Texas at Dallas, Richardson, TX, USA

[26]Melbourne School of Psychological Sciences, University of Melbourne, Melbourne, VIC, Australia

[27]Turner Institute for Brain and Mental Health, Monash University, Clayton, VIC, Australia

[28]Healthy Brain and Mind Research Centre, Neuroscience of Addiction and Mental Health Program, Australian Catholic University, Fitzroy, VIC, Australia; Clinical Psychopharmacology Unit, Research Department of Clinical, Educational and Health Psychology, University College London, London, UK

[29]Faculty of the Arts, Social Sciences and Humanities, School of Psychology, Wollongong, Australia, University of Wollongong, Wollongong, NSW, Australia

[30]Department of Psychiatry & Psychology, Hospital Clínic, Institut d'Investigacions Biomèdiques August Pi i Sunyer (IDIBAPS), Centro de Investigación en Red de Salud Mental (CIBERSAM), Barcelona, Spain

[31]Department of Psychiatry, University Medical Center Utrecht Brain Center, Utrecht University, Utrecht, The Netherlands

[32]Neuroscience of Addiction Lab, Center for Substance Use and Addiction Research, Department of Psychology, Education & Child Studies, Erasmus School of Social and Behavioral Sciences, Erasmus University Rotterdam, Rotterdam, The Netherlands

[33]FIDMAG Germanes Hospitalàries Research Foundation, Barcelona, Spain

[34]Instituto de Neurobiología, Universidad Nacional Autónoma de México (UNAM) campus Juriquilla, Querétaro, Mexico

[35]Department of Psychiatry, McGill University, Montreal Neurological Institute, Montreal, QC, Canada

[36]Neuroimaging Research Branch, National Institute on Drug Abuse (NIDA), National Institutes of Health, Baltimore, MD, USA

[37]Vrije Universiteit Brussel (VUB), Universitair Ziekenhuis Brussel (UZ Brussel), Department of Psychiatry, Brussels, Belgium

[38]Department of Clinical Neuropsychology, Faculty of Behavioural and Movement Sciences, Vrije Universiteit Amsterdam, Amsterdam, The Netherlands

[39]Department of Clinical Psychology, School of Psychology, Monash University, Melbourne, VIC, Australia

[40]Department of Neuroscience, University of Rochester Medical Center, Rochester, NY, USA

[41]Clinic of Psychiatry and Psychotherapy, Psychiatric Services Aargau, Windisch, Switzerland

[42]Department of Psychiatry (UPK), University of Basel, Basel, Switzerland

[43]Division of Psychiatry, Department of Brain Sciences, Faculty of Medicine, Imperial College London, London, UK

[44]Department of Psychiatry, Oregon Health & Science University, Portland, OR, United States

[45]Department of Psychiatry and Biobehavioral Sciences, Semel Institute for Neuroscience and Human Behavior, University of California, Los Angeles, CA, USA

[46]First Affiliated Hospital of Anhui Medical University, Hefei, China

[47]Neuroscience Center Zurich, University of Zurich & ETH Zurich, Switzerland

[48]University Hospital for Psychiatry, Psychotherapy and Psychosomatics, Halle (Saale), Germany

[49]Division of Addiction Psychiatry, Department of Psychiatry, University Hospitals of Geneva, Geneva, Switzerland

[50]Faculty of Medicine, University of Geneva, Geneva, Switzerland

[51]Montreal Neurological Institute, McGill University, Montreal, QC, Canada

[52]Imaging Genetics Center, Mark & Mary Stevens Neuroimaging and Informatics Institute, Keck School of Medicine, University of Southern California, Marina del Rey, CA, USA

[53]Department of Psychiatry, University of Vermont College of Medicine, Burlington, VT, USA

[54]Institute for Neuroscience and Medicine (INM-7), Forschungszentrum Jülich, 52425 Jülich, Germany

[55]Max Planck Institute for Human Cognitive and Brain Sciences, 04103 Leipzig, Germany

[56]Max Planck School of Cognition, 04103 Leipzig, Germany

[57]Institute of Systems Neuroscience, Medical Faculty and University Hospital Düsseldorf, Heinrich Heine University Düsseldorf, 40225 Düsseldorf, Germany

Abstract

Substance use disorders (SUD) are chronic conditions with devastating effects on brain health, functioning, and survival. In this study, we compared brain morphometry of 2,782 individuals with SUD to 1,951 controls and assessed the topographic overlap of these differences with brain connectivity and receptor architecture. Across SUD, we identified a morphometric signature involving frontal, parietal, temporal and limbic systems that overlapped with cortical hub regions and harbored cortical and subcortical disease epicenters. Findings were highly consistent across six substances and numerous robustness and generalizability analyses. Transdiagnostic comparisons showed high spatial overlap of SUD epicenters with those of schizophrenia and bipolar disorder, suggesting shared network-constrained cortical differences. Finally, multivariate mapping revealed that SUD brain differences aligned with two neurotransmitter axes contrasting cannabinoid-opioid and dopaminergic systems. These findings indicate that addiction-related brain differences are shaped by connectome and neurotransmitter architecture, positioning brain network and neurochemical organization as key principles of SUD-related brain alterations.

Introduction

Substance use disorders (SUD) are a major and growing global health concern, affecting millions of individuals worldwide, contributing substantially to the overall burden of mental illness[1,2]. SUD are understood to arise from a multifactorial interplay between environmental factors and biological vulnerability, including genetic risk[3,4]. Converging evidence from neuroimaging, neuropathological and molecular studies has identified consistent differences in brain structure and function associated with SUD[5–7]. Large-scale MRI case–control studies from the ENIGMA Addiction Working Group have demonstrated robust cortical and subcortical morphometric differences, as well as altered cortical and subcortical structural asymmetry, across multiple substances, including alcohol, cocaine, cannabis, nicotine, and amphetamines[8,9]. These alterations involve brain systems implicated in reward processing, salience attribution, learning and cognitive control[10,11].

Importantly, structural differences have been linked to both the stage and the severity of addiction, with converging evidence indicating a dose–response relationship between cumulative substance exposure and macroscopic neuroanatomical differences; for example, progressively lower cortical thickness, smaller subcortical volumes, reduced white-matter integrity, and advanced brain-age, with the strongest evidence in alcohol and cocaine use[12–17], extending to amphetamines, cannabis, nicotine, and opioids[18–20]. Mechanistically, these patterns plausibly reflect combined neurotoxic and neuroimmune processes such as neuronal injury, white matter compromise, microvascular damage, and neuroinflammation[21–23], moderated by genetic liability and early-life adversity[6,24].

Despite this growing evidence, the principles that organize the spatial distribution of SUD-related morphometric differences remain poorly understood. Prior work has shown that structural abnormalities in brain disorders are not random but spatially coordinated, reflecting the brain's intrinsic organizational architecture[25–29]. This raises the question of whether network-based models of brain connectivity can explain why some regions are more affected than others in SUD.

Two complementary models from network neuroscience are particularly relevant. The hub vulnerability hypothesis proposes that hub regions, i.e., highly interconnected brain regions that are central for information integration and characterized by high metabolic costs, are disproportionately susceptible to damage[30–33]. Evidence for this model first emerged in neurodegenerative disorders, where hub regions such as the posterior cingulate cortex and precuneus were shown to be preferentially affected in Alzheimer's disease[34]. Subsequent studies extended this principle to psychiatric disorders, including schizophrenia[26]. In addition to cortical hubs, current circuit models of addiction emphasize that dysregulated communication between limbic/striatal hubs and prefrontal control regions underlies compulsive drug seeking and impaired self-regulation, underscoring the relevance of subcortico-cortical connectivity[35,36]. The epicenter model posits that pathological processes

can be traced back to specific regions acting as epicenters; epicenters are regions whose normative connectivity profile matches the observed spatial distribution of structural differences, with spread proposed to occur along connected pathways[28,33,37]. Initially developed in neurodegenerative disorders[38] such as Parkinson's[39] and Alzheimer's disease and frontotemporal dementia[40], this framework has since been extended to epilepsy and examined in psychiatric disorders[25–27,41–43].

A distinct feature of SUD neuropathophysiology is that neurobiology interacts with the effects of substances, mediated by the brain's neurochemical architecture[6]. Psychoactive substances act on distinct neurotransmitter receptor systems, whose cortical distribution is closely aligned with the brain's network topology[44,45]. These receptor landscapes could plausibly act as molecular scaffolds that constrain the spread of pathology along functional circuits. Yet the principles organizing the spatial distribution of morphometric differences in addiction, and the extent to which network connectivity and neurochemical architecture jointly constrain these patterns, remain to be established.

Here, we integrate these network and molecular perspectives to test the hypothesis that structural brain differences in SUD are shaped by normative connectivity and neurotransmitter receptor distributions (**Fig. 1**). Using structural brain MRI data from 2,782 individuals with SUD and 1,951 healthy controls from the ENIGMA Addiction Working Group, we (i) characterized morphometric differences across individuals with SUD and within each of six substance use categories, (ii) tested whether these differences preferentially affect hubs as well as whether they follow the connectivity profiles of specific epicenter regions, (iii) examined cross-disorder similarity with other major psychiatric conditions, and (iv) linked SUD-related morphometric difference patterns to PET-based neurotransmitter receptor distributions derived from 20 neurotransmitters (e.g., dopamine, serotonin, GABA, acetylcholine, opioid, and histamine systems). We further performed complementary robustness and individual-level analyses to confirm the stability and generalizability of our findings.

Results

Structural differences across SUD

We compared structural neuroimaging data from 2,782 individuals with at least one SUD and 1,951 healthy controls across 51 international sites of the ENIGMA Addiction Working Group (**Fig. 2a**; Supplementary **Table S1**). 3D T1-weighted MRI scans were processed locally with FreeSurfer[46,47] using the Desikan–Killiany atlas[48] to extract cortical thickness (CT) and subcortical volumes (SV). Site-related variance was harmonized using ComBat[49,50], and region-wise linear regression models included diagnosis, age, sex, and intracranial

volume. Effect sizes and FDR-corrected statistics were computed for the overall SUD group and each substance-specific cohort (Supplementary **Tables S2–S3**).

Across the cortex, individuals with SUD showed widespread lower cortical thickness relative to healthy controls (**Fig. 2b**; Supplementary **Table S4**). After FDR correction, 65 of 68 cortical regions showed significant reductions ($p_{FDR} < 0.05$), with the largest effects in frontal, parietal, and temporal regions, including the left superior frontal gyrus (Cohen's $d = -0.33$), left caudal middle frontal gyrus (Cohen's $d = -0.31$), and right inferior parietal cortex (Cohen's $d = -0.29$). Subcortically, 11 of 14 structures showed lower values with the strongest effect sizes in the hippocampus (−0.25/−0.24) and amygdala (−0.24/−0.21) (**Fig. 2b**; Supplementary **Table S5**). Effect size patterns were robust to alternative age specifications, with inclusion of a quadratic age term having negligible impact (see Supplementary Methods). These findings are consistent with and extend previous large-scale analyses[8,51,52].

Beyond these main effects, SUD-related structural differences interacted with ageing, with more pronounced cortical, but not subcortical, case–control differences at older ages, consistent with age-dependent or cumulative effects (**Fig. 2c**; Supplementary **Tables S20–S21**). Effects of biological sex were comparatively subtle and localized to subcortical regions (**Fig. 2d**; Supplementary **Tables S23–S24**).

Finally, to assess robustness of the combined-SUD phenotype and ensure results were not driven by any single substance, we conducted a leave-one-out analysis excluding each of the six SUD subtypes in turn. The spatial topography of cortical and subcortical differences remained consistent across iterations (Supplementary **Tables S6–S7**) as reflected by high spatial correlations between leave-one-out effect size maps (Supplementary **Tables S8–S9**). Further details are provided in the Supplementary Results.

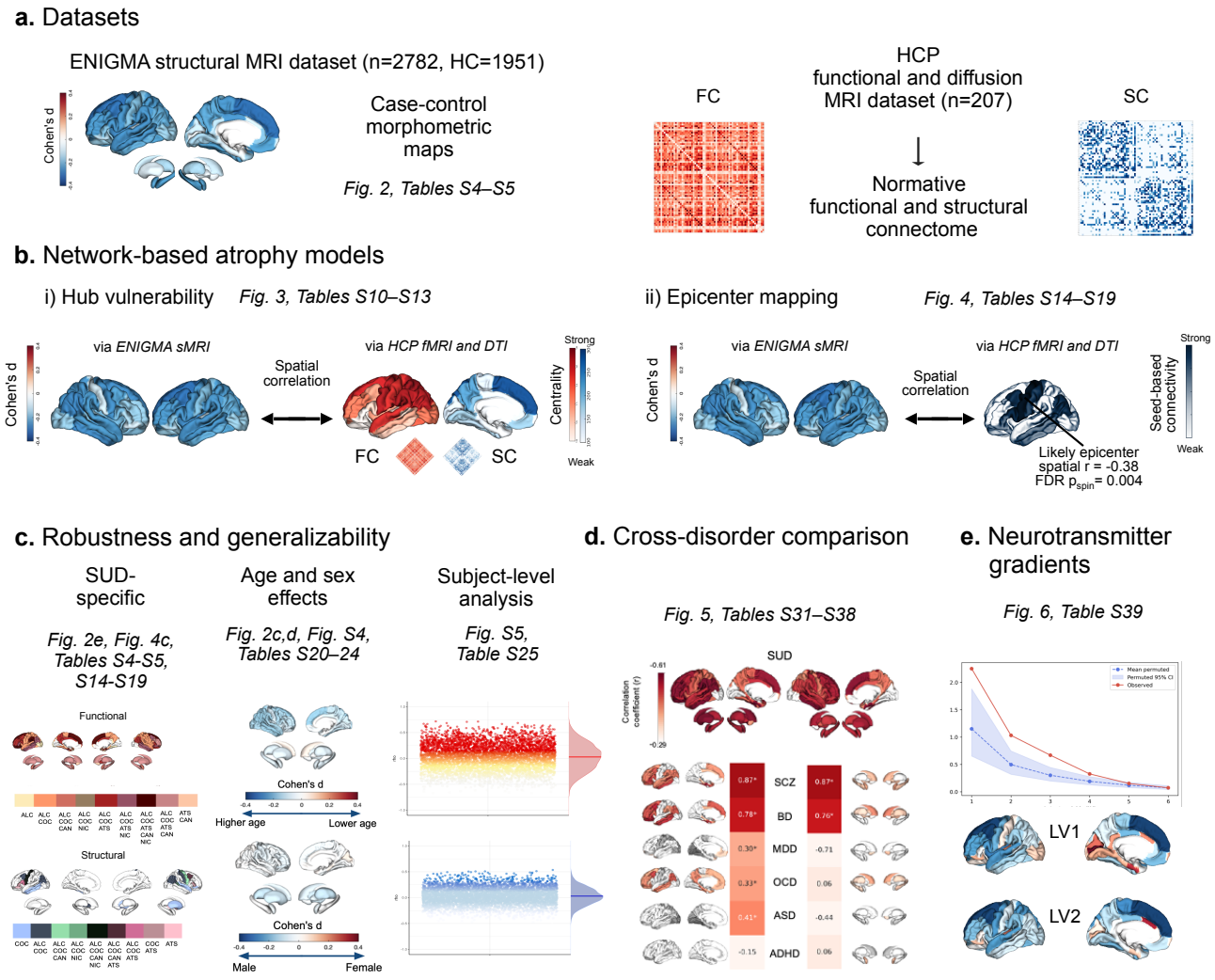

Fig. 1. Overview of the datasets and analysis pipeline. (**a**) ENIGMA Addiction Working Group structural MRI dataset (n = 2,782 individuals with SUD and n = 1,951 healthy controls), including six substance categories: alcohol, amphetamines, cocaine, cannabis, nicotine, and opioids. Case–control cortical thickness and subcortical volume alteration maps were generated for each substance category and for the combined SUD group. (**b**) Normative functional and structural connectomes from the Human Connectome Project (n = 207) were used to test two network-based models of SUD-related brain alterations: hub vulnerability and epicenter mapping. (**c**) Robustness and generalizability analyses, including substance-specific profiles, SUD-by-age, SUD-by-sex interaction effects, and subject-level analyses. (**d**) Cross-disorder comparisons of SUD-related maps with those from schizophrenia, bipolar disorder, major depressive disorder, obsessive-compulsive

disorder, autism spectrum disorder, and attention-deficit/hyperactivity disorder. (**e**) Association of neurotransmitter density with cortical alterations and the connectome organization in SUD.

SUD-specific structural differences

Of the 2,782 individuals with SUD, 2,312 had a single SUD diagnosis (i.e., no comorbid SUD) and were included in substance-specific analyses (alcohol: 902; amphetamines: 178; cannabis: 286; cocaine: 278; nicotine: 600; opioids: 68). Each group was compared with the pooled healthy control sample (n = 1,951). Substance-specific analyses revealed heterogeneous but substantially overlapping morphometric difference patterns (**Fig. 2e**; Supplementary **Tables S4–S5**).

Lower cortical thickness was most pronounced in alcohol use disorder (peak Cohen's $d = -0.47$), followed by cocaine (−0.34), with nicotine (−0.28) showing intermediate effects that were less consistent across regions. Subcortical differences followed a similar ranking, with alcohol showing the most consistent volume reductions across nearly all subcortical structures (peak Cohen's $d = -0.34$), followed by nicotine (−0.24). Cannabis use was associated with more circumscribed, limbic-predominant reductions, particularly in the hippocampus (−0.27) and amygdala. In contrast, amphetamine- and opioid-related effects did not survive FDR correction and were limited to small, non-significant trends (**Fig. 2e**; Supplementary **Tables S4-S5**).

Overall, substance-specific brain morphometric differences showed highly similar spatial patterns, as evidenced by strong intercorrelations of effect sizes and confirmatory principal component analyses (Supplementary **Fig. S2a–b**).

a. Demographics

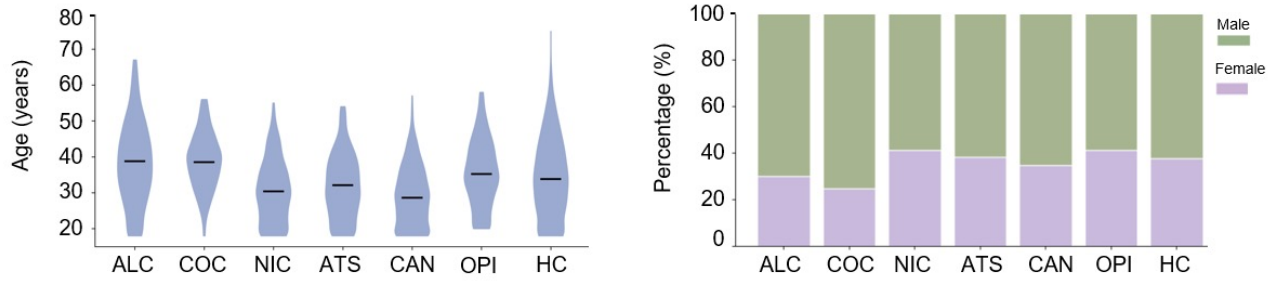

b. Morphometric differences across all SUD

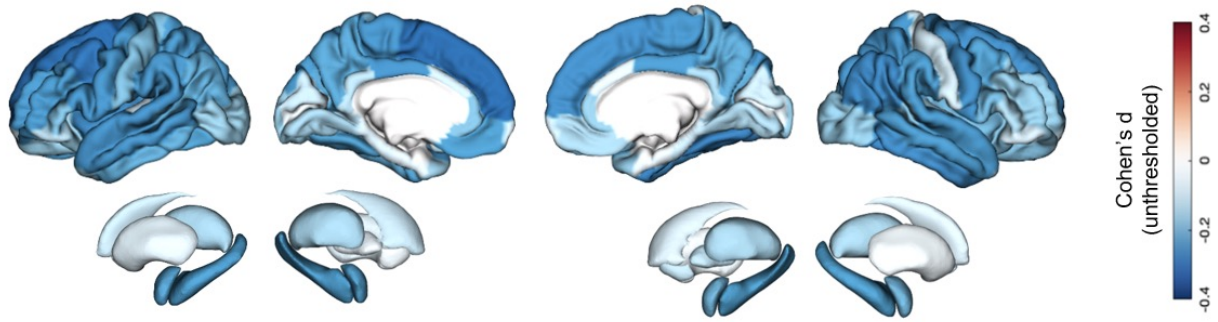

c. Age by SUD interaction effects

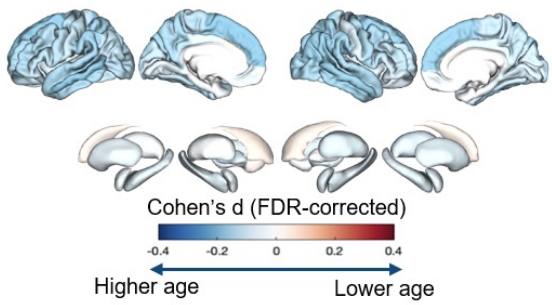

d. Sex by SUD interaction effects

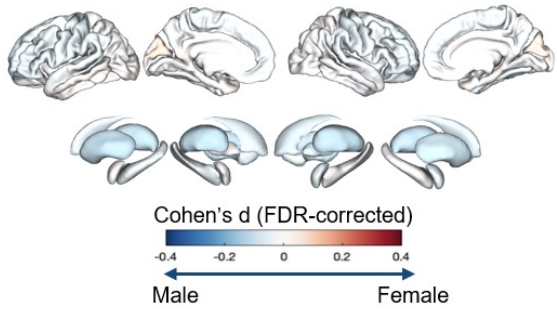

e. Morphometric differences of specific SUD

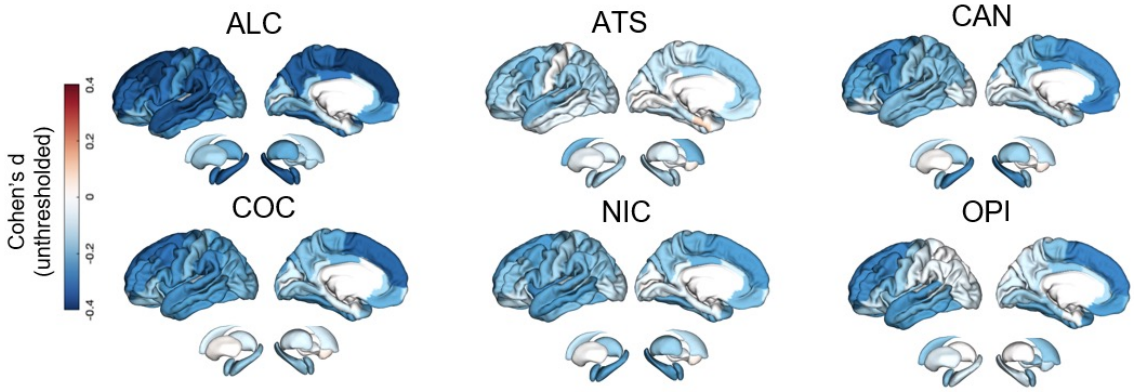

Fig. 2. Morphometric differences in SUD. (**a**) Demographic characteristics of all groups. Age distributions are shown as mean ± SD (*n*) for controls and for individuals with a primary substance use disorder diagnosis (SUD): controls 33.8 ± 12.0 (*n* = 1951), alcohol 38.8 ± 12.0 (*n* = 902), cocaine 38.5 ± 8.4 (*n* = 278), nicotine 30.4 ± 9.8 (*n* = 600), amphetamines 32.1 ± 10.1 (*n* = 178), cannabis 28.6 ± 9.2 (*n* = 286), and opioids 35.2 ± 9.8 (*n* = 68). Sex distributions (percentage female) were: controls 37.5%, alcohol 30.0%, cocaine 24.8%, nicotine 41.3%, amphetamines 38.2%, cannabis 34.6%, and opioids 41.2%. For more details, see Supplementary **Table S2**. (**b**) Unthresholded effect size maps of morphometric differences across the combined SUD phenotype, showing changes in cortical thickness and subcortical volume as quantified by Cohen's *d* (see Supplementary **Tables S4–S5**). (**c**) FDR-corrected maps of SUD-by-age interaction effects across the combined SUD phenotype, showing which cortical and subcortical regions are more severely affected in older versus younger individuals (see Supplementary **Tables S20–S21)**. (**d**) FDR-corrected maps of SUD-by-sex effects across all SUD categories, showing which cortical and subcortical regions are more severely affected in male versus female individuals (see Supplementary **Tables S23–S24)**. (**e**) Unthresholded effect size maps of morphometric differences in specific SUD categories (alcohol, amphetamines, cannabis, cocaine, nicotine, opioids) for cortical thickness and subcortical volume, illustrating substance-specific variations in effect magnitude on a shared spatial topography (see Supplementary **Tables S4–S5**).

Functional and structural degree centrality predict regional susceptibility in SUD

According to the hub vulnerability hypothesis, brain regions with high topological centrality (hubs)[30] are disproportionately susceptible to biological insults due to their central role in information integration, long-range communication, and high metabolic demands[53]. We tested whether the magnitude of regional morphometric differences identified in our mega-analysis (**Fig. 2b**; Supplementary **Tables S4–S5**) correlated with each region's network centrality (Fig. 3a).

Regional functional and structural centrality were derived from cortical and subcortico-cortical connectivity measurements of an independent normative sample (**Fig. 3a**)[54,55].

Cortical regions exhibiting higher functional and structural centrality showed significantly lower cortical thickness in the combined SUD map (r_{func} = –0.51, p_{spin} = 0.002; r_{struc} = –0.49, p_{spin} < 0.0001; **Fig. 3b**; Supplementary **Table S10**). In contrast, subcortical volume reductions were not significantly associated with subcortico-cortical degree centrality (both $p_{shuf} \geq 0.17$; Supplementary **Table S11**).

Substance-specific hub vulnerability

We next examined whether the observed relationship between brain network centrality and morphometric

differences in SUD varied across substance categories (**Fig. 2e**). Alcohol, cocaine, and amphetamine use disorders showed significant negative correlations between cortical thickness and both functional and structural degree centrality (all $r < -0.30$, FDR-$p_{spin} < 0.05$**; Fig. 3c**), whereas nicotine and cannabis showed significant associations with structural centrality only (all $r_{struc} < -0.30$, FDR-$p_{spin} < 0.05$**; Fig. 3c**; Supplementary **Tables S10–S11**). Corresponding associations between subcortico-cortical degree centrality and subcortical volume differences were non-significant across substances (Supplementary **Table S11**). Overall, cortical hub vulnerability was robust across SUD and consistent across centrality metrics (Supplementary **Tables S12–S13**), whereas subcortico-cortical hub vulnerability was not significant. Further details are provided in the Supplementary Results.

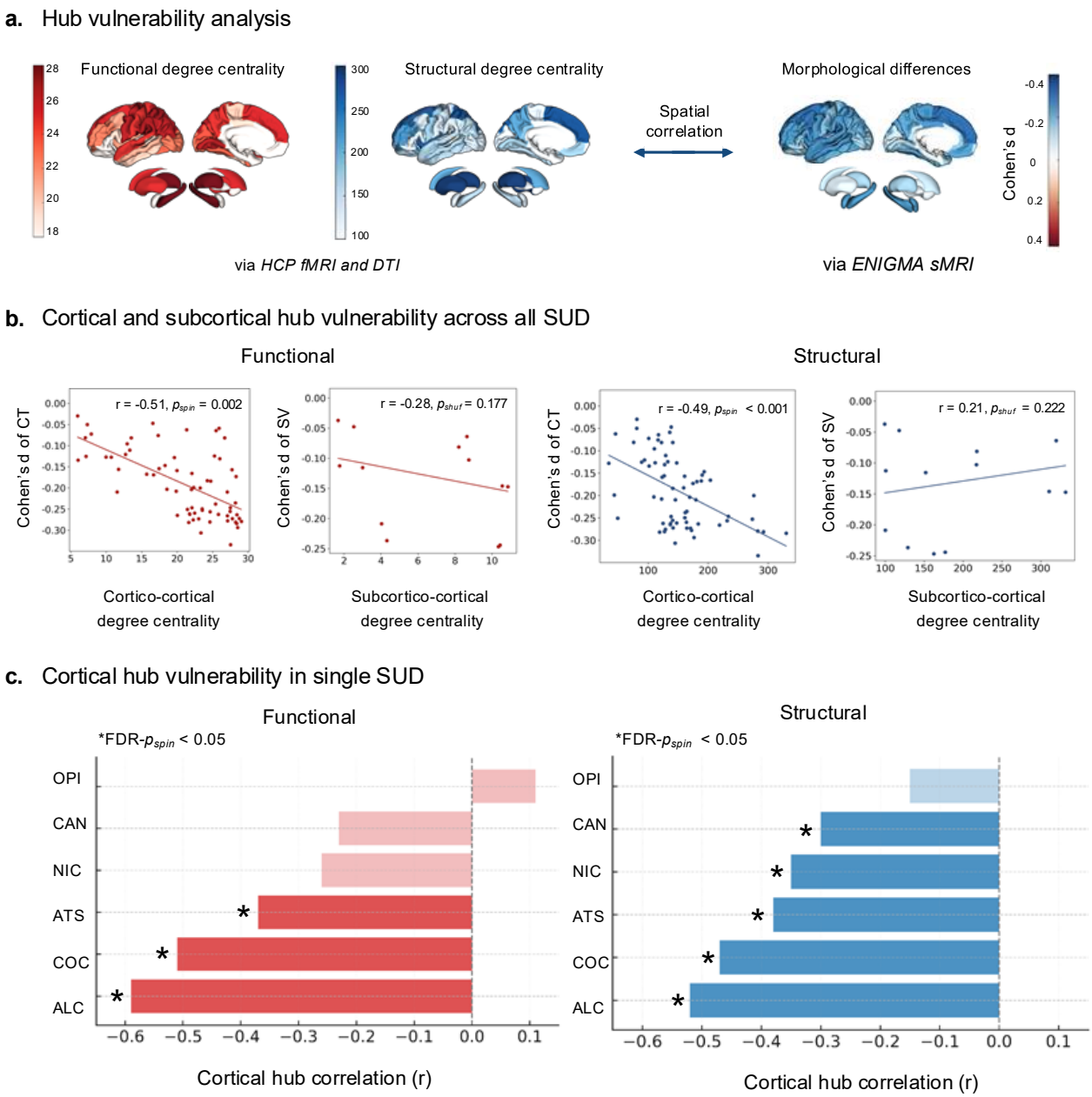

Fig. 3. Hub vulnerability in functional and structural connectivity in SUD. (a) Left: HCP-derived normative functional and structural centrality, showing degree centrality for both functional and structural connectivity. Right: mega-analytic SUD morphometric map from our analysis. **(b)** Correlation plots show the spatial relationship between cortical thickness and subcortical volume differences (Cohen's *d*) in the combined SUD phenotype and normative degree centrality, shown separately for functional vs structural and cortico-cortical vs subcortico-cortical connectivity. **(c)** For each single SUD, separate bar plots illustrate spatial

correlations between cortical thickness differences (Cohen's *d*) and HCP-derived functional (left, red) and structural (right, blue) cortico-cortical degree centrality. Cortical spatial correlations were assessed using spin-permutation tests (10,000 repetitions) to correct for spatial autocorrelation[56]. Subcortical spatial correlations were assessed by randomly shuffling subcortical labels (10,000 repetitions). Statistical significance (FDR-p_{spin} < 0.05) is denoted by bar color; faded color denotes non-significant correlation.

Disease epicenters of SUD

Beyond the preferential involvement of highly connected hubs, network models of brain disorders suggest that spatially distributed structural alterations may reflect the connectivity profiles of specific regions that act as candidate epicenters, anchoring disease-related patterns across large-scale circuits[26,37,41]. To identify such candidate epicenters underlying morphometric differences in substance use disorders, we performed seed-based epicenter mapping using normative functional and structural connectivity profiles of each region. Regions whose normative functional or structural connectivity profiles showed significant spatial correlations with the regional morphometric difference maps (Cohen's *d*; FDR-p_{spin} < 0.05) were considered epicenters, suggesting that these regions may constrain the observed spatial distribution of lower cortical thickness in SUD (**Fig. 4a**). We identified several functional cortical epicenters, forming a distributed network involving medial temporal and orbitofrontal regions, with additional extensions into frontoparietal cortices, including the lateral orbitofrontal, entorhinal, inferior temporal, and banks of the superior temporal sulcus (**Fig. 4b**; Supplementary **Table S14**). By contrast, structural cortical epicenters were more circumscribed, with the strongest associations observed predominantly in sensorimotor and adjacent frontoparietal regions, including the precentral, postcentral, and paracentral gyri (**Fig. 4b**; Supplementary **Table S14**). Subcortical epicenters primarily involved the hippocampus, amygdala, and striatal regions (**Fig. 4b**; Supplementary **Table S15**).

Similarity structure of substance-specific epicenter maps

Using substance-specific Cohen's *d* maps, we identified epicenters for each single SUD (Supplementary **Fig. S3**) and quantified their spatial similarity to the combined SUD epicenter profile. Cortical epicenter maps showed high concordance with the combined SUD epicenters across substances, with the highest similarity observed for alcohol and cocaine (all $r > 0.82$; FDR-p_{spin} < 0.05; Supplementary **Table S16**). At the subcortical level, cross-correlation analyses revealed greater variability in subcortical epicenter patterns across substances (Supplementary **Table S17**). Overall, opioid use disorder showed the lowest similarity across both cortical and subcortical modalities, likely reflecting limited sample size ($n = 68$).

Given this high overall concordance, we examined the overlap and uniqueness of epicenters across substances (**Fig. 4c**). Across functional and structural cortical maps, epicenters shared by multiple substances largely overlapped with regions showing the highest epicenter likelihood in the combined SUD map (**Fig. 4b**), including frontal, parietal, and lateral temporal association areas. Substance-specific epicenters were comparatively sparse and modality-dependent, with distinct cortical loci for alcohol, cocaine, and cannabis, and limited subcortical specificity (**Fig. 4c**; Supplementary **Tables S18–S19**). Together, these results reveal a core set of frontal, parietal, and temporal epicenters anchoring cortical vulnerability across substances, alongside more circumscribed substance-specific loci reflecting variation in network-constrained morphometric differences. Further details are provided in the Supplementary Results.

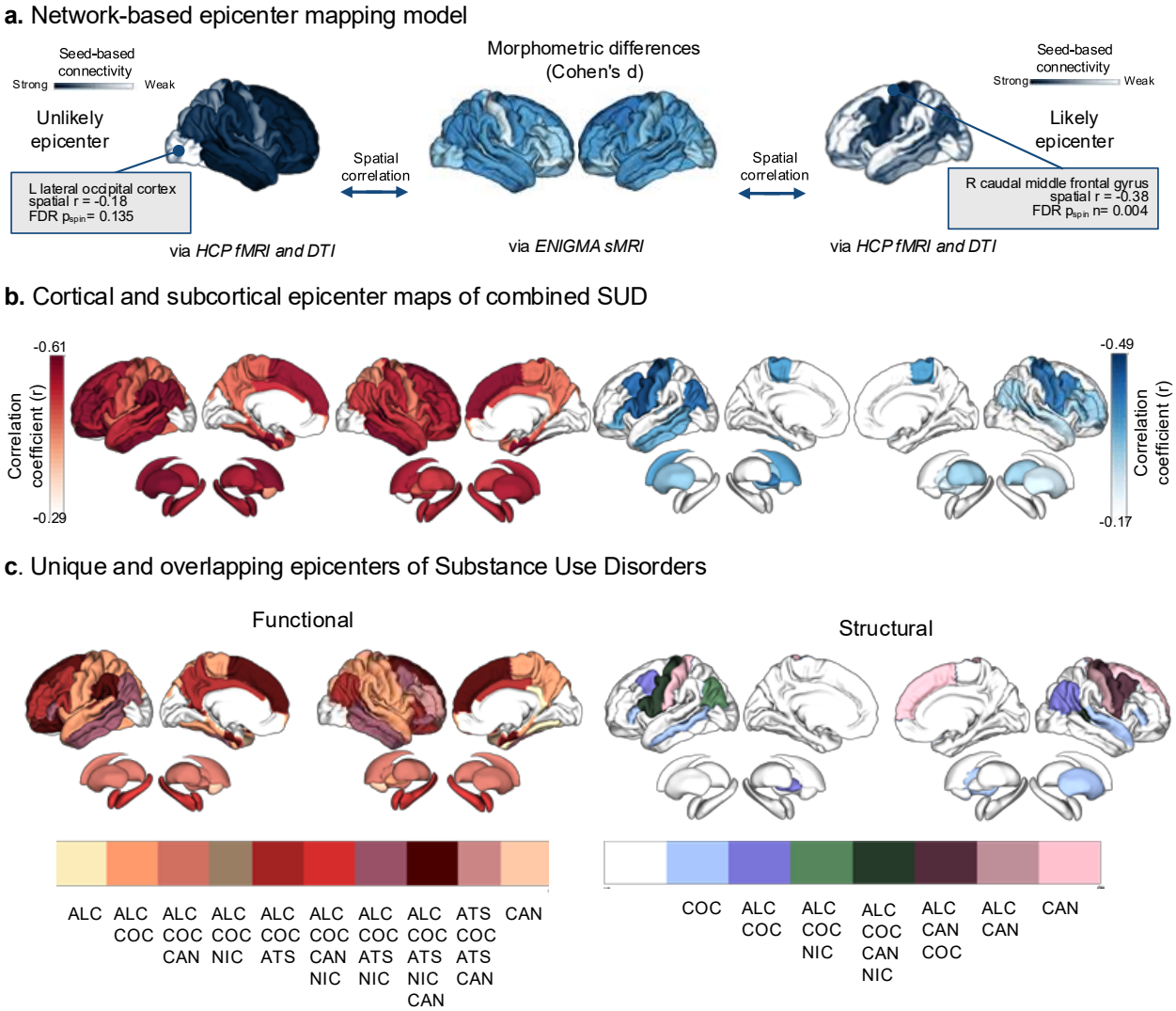

Fig. 4. Functional and structural epicenters in SUD. (a) Model of network-based epicenter mapping. Spatial correlation between normative connectivity profiles and observed SUD-related cortical differences is used to identify likely versus unlikely epicenters. **(b)** Cortical and subcortical epicenter maps of the combined SUD pattern, derived from spatial correlations between normative functional (left) or structural (right) connectivity and cortical thickness differences in SUD. Darker colors indicate higher epicenter likelihood (Pearson's r). Only regions showing significant spatial correlation with the maps of morphometric difference (Cohen's *d*, FDR-$p_{spin} < 0.05$, 10,000 repetitions) are displayed as putative cortical or subcortical epicenters. **(c)** Overlap of functional and structural epicenters across substances. Shared epicenters are visualized as darker (more extensive overlap) and highlight regions which are shared epicenters, whereas unique epicenters are visualized lighter and highlight substance-specific epicenters. Only epicenters surviving spin-permutation testing (10,000 repetitions) and multiple-comparison correction are displayed (FDR-$p_{spin} < 0.05$).

Robustness and generalizability analyses

Interaction of SUD diagnosis with age and sex

Given known age[57–60] and sex-related effects[61–63] on brain structure in psychiatric disorders[64,65] and SUD[66,67], we tested SUD-by-age and SUD-by-sex interactions on cortical and subcortical morphology and evaluated whether these effects conformed to the hub vulnerability and epicenter hypotheses.

Significant SUD-by-age interactions were observed across multiple cortical thickness regions, whereas no such interactions were detected subcortically, indicating greater age-related case–control divergence in cortical regions (**Fig. 2c**; Supplementary **Tables S20–S21**).

Cortical regions showing SUD-by-age interaction effects were significantly correlated with functional ($r = -0.68$, $p_{spin} < 0.001$) and structural ($r = -0.42$, $p_{spin} < 0.001$) degree centrality (Supplementary **Fig. S4a**). Epicenter mapping of SUD-by-age effects revealed strong correlations with functional and structural epicenter maps derived from the combined SUD Cohen's *d* pattern (Supplementary **Fig. S4b**; *regional age-sensitivity* detailed in Supplementary **Table S22**). Together, these findings indicate that age-related cortical decline in SUD follows hub vulnerability and epicenter patterns similar to those observed for cross-sectional morphometric differences.

No significant SUD-by-sex interactions were observed across cortical regions (all $p_{spin} > 0.05$; **Fig. 2d**; Supplementary **Table S23**). Subcortically, significant SUD-by-sex interactions were limited to bilateral putamen and thalamus (Supplementary **Table S24**). Accordingly, hub and epicenter analyses were not further applied to sex effects.

Individual-level validation of hub vulnerability and epicenter mapping

To assess the sensitivity of group-level findings, we repeated analyses at the individual participant level. Consistent hub vulnerability and region-wise epicenter frequency patterns were observed in SUD patients, albeit with reduced sensitivity reflecting increased inter-individual variability (Supplementary **Fig. S5**; Supplementary **Table S25**).

Robustness of SUD-specific morphometric differences to age distribution

To test whether the larger alcohol and cocaine effects were driven by older age distributions (**Fig. 2a**), we repeated the case–control bootstrap analysis (~60% resampling without replacement), applying weighted resampling toward a lower target mean age for alcohol and cocaine groups (**Fig. S6**; Supplementary **Tables S26–S27**). Under age-harmonized resampling, alcohol and cocaine remained the largest cortical effects (median $d > -0.19$), and alcohol remained the largest subcortical effect, indicating that higher effect magnitudes were not explained solely by age distribution or SUD-by-age interaction effects.

Robustness of regional SUD-specific morphometric patterns to sample size

To ensure that substance-specific morphometric differences were not artifacts of unequal sample sizes, we repeated analyses using bootstrap resampling with equalized *n* across substances. Median effect sizes remained stable in magnitude and direction across resampled datasets, with confidence intervals narrowing at larger n (Supplementary **Fig. S7**). Bootstrap-derived effect-size maps showed increasing similarity to full-sample reference maps as sample size increased, supporting robust and reproducible substance-specific morphometric patterns (Supplementary **Fig. S8**).

Robustness of SUD-specific brain morphometric differences to control sample

Finally, we tested robustness to control-sample composition by repeating analyses using study-specific healthy control groups instead of the pooled control cohort (Supplementary **Fig. S9**; Supplementary **Tables S28–S30**). Across comparison strategies, substance-specific maps showed high spatial correspondence (r = 0.67–0.99), with modestly reduced similarity for substances with smaller control samples. Together, these analyses demonstrate that observed morphometric differences are robust to sample-size variation and control-group composition.

Transdiagnostic disorder comparison

Having established the robustness of the SUD epicenter architecture, we next examined the extent to which these patterns are shared across major psychiatric disorders, comparing SUD epicenters with those of six

disorders using ENIGMA meta-analytic maps[68]. Meta-analytic case–control maps from six major psychiatric disorders were used to generate epicenter maps for schizophrenia[69,70], bipolar disorder[71,72], major depressive disorder[73,74], obsessive-compulsive disorder[75,76], attention-deficit/hyperactivity disorder[77,78], and autism spectrum disorder[79] (Supplementary **Tables S31–S34**).

Across cortical and subcortical domains, SUD epicenters showed strongest spatial correspondence with schizophrenia and bipolar disorder in both functional and structural modalities (r = 0.55–0.87, $p_{spin} \leq 0.047$; **Fig. 5a**; Supplementary **Tables S35–S36**). Correlations with obsessive-compulsive disorder, attention-deficit/hyperactivity disorder, and autism spectrum disorder were comparatively weaker. Major depressive disorder showed a distinct pattern, characterized by a robust inverse association with subcortical functional epicenters ($r = -0.71$, $p_{spin} = 0.011$; Supplementary **Table S36**). Substance-specific epicenter profiles largely recapitulated these transdiagnostic trends, while also revealing substance-dependent deviations, most prominently for opioids, which showed particularly strong correspondence with major depressive disorder.

To further characterize the anatomical basis of this convergence, we examined regional epicenters showing spatial overlap across SUD and the six psychiatric disorders. In line with strong transdiagnostic correlations, functional epicenters were predominantly shared between SUD, schizophrenia, and bipolar disorder, involving frontotemporal and parietal cortices, as well as bilateral caudate nuclei and the left putamen (**Fig. 5b**; Supplementary **Tables S37–S38**). A limited number of regions, including the left frontal pole and right temporal pole, also overlapped with major depressive disorder. In contrast, overlap of structural epicenters was sparse and largely restricted to frontoparietal cortical regions shared between SUD, schizophrenia, and bipolar disorder. No cortical or subcortical epicenter overlap was observed with obsessive-compulsive disorder, attention-deficit/hyperactivity disorder, or autism spectrum disorder (**Fig. 5b**; Supplementary **Tables S37–S38**). Further details are provided in the Supplementary Results.

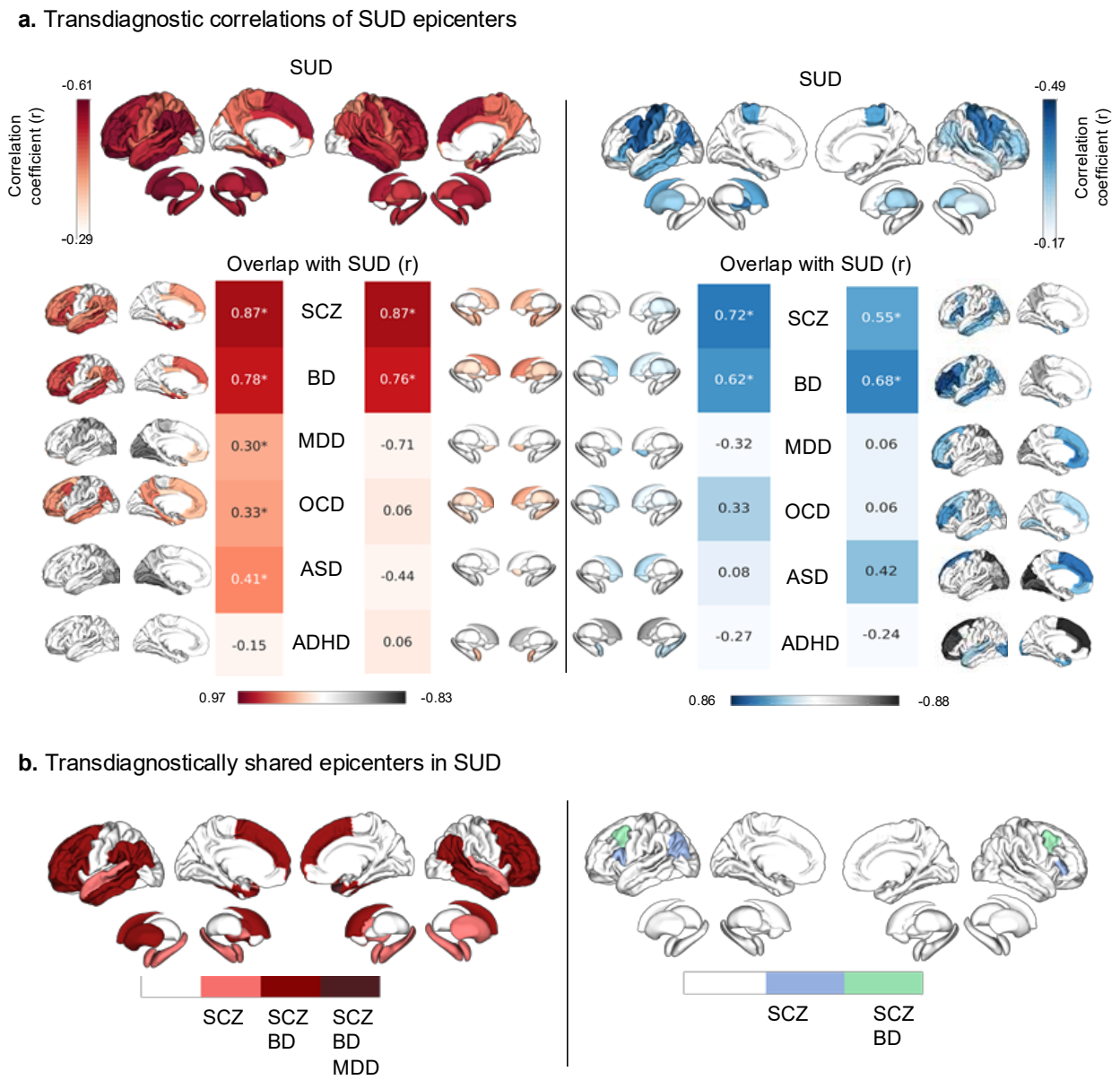

Fig. 5. Correlations between SUD and psychiatric disorders. (a) top: SUD epicenter map. Bottom: Spatial correlations of SUD cortical and subcortical epicenter maps and each psychiatric disorder (schizophrenia, bipolar disorder, major depressive disorder, obsessive-compulsive disorder, attention-deficit/hyperactivity disorder, and autism spectrum disorder), shown separately for functional and structural modalities. For visualization purposes, epicenter maps for the remaining psychiatric disorders are shown without multiple-testing correction ($p_{spin} < 0.05$), to illustrate overall pattern similarity rather than individual epicenters. **(b)** Brain map of shared and disorder-specific epicenters across SUD and the six psychiatric disorders, showing overlap

in both functional and structural connectivity. Shared and unique epicenters represent regions surviving multiple-testing correction (FDR-$p_{spin} < 0.05$).

Association of neurotransmitter density with cortical differences and epicenters in SUD

Endogenous neurotransmitter systems are key mediators of exogenous substance effects[6,35] and are closely linked to large-scale brain network architecture[44,45]. Building on evidence for network-level involvement in SUD, we examined the relationship between neurotransmitter receptor distribution, SUD-related cortical differences, and intrinsic connectivity organization. We applied partial least squares (PLS) analysis to relate regional neurotransmitter receptor density profiles[44] (Supplementary **Table S39**) to the patterns of substance-specific cortical thickness differences (**Fig. 2e**; Supplementary **Table S4**). The decomposition revealed four statistically significant latent variables (LVs; permutation $p < 0.05$, **Fig. 6a**), with the first two explaining nearly 90% of the cross-covariance (LV1 = 75.5%, LV2 = 15.9%; **Fig. 6b**). Both LV1 and LV2 aligned with the distributed cortical difference pattern (**Fig. 6c**). LV1 emphasized frontotemporal vulnerability, whereas LV2 additionally captured parietal involvement; both patterns correlated strongly with the combined SUD morphometric difference map (LV1 $r = 0.97$, $p_{spin} < 0.001$; LV2 $r = 0.86$, $p_{spin} < 0.001$). The primary axis of covariance (LV1; 75.5%) indicated that regions with the greatest morphometric differences exhibited higher normative density of KOR, mGluR5, CB1, H3, and MOR (all loadings z-scores > 1.96; **Fig. 6d**). The second axis (LV2; 15.9%) indicated that these regions were, to a lesser extent, characterized by lower normative density of D1, VAChT, DAT, and NMDA (all loadings z-scores < −1.96; **Fig. 6d**). Importantly, both LVs were constrained by normative connectome architecture and correlated negatively with functional centrality (LV1 $r = -0.37$, $p_{spin} = 0.018$; LV2 $r = -0.51$, $p_{spin} = 0.002$) and structural centrality (LV1 $r = -0.43$, $p_{spin} = 0.001$; LV2 $r = -0.48$, $p_{spin} < 0.001$; **Fig. 6e**). This indicates partial convergence between the spatial pattern of the SUD morphometric differences, neurotransmitter-defined vulnerability axes, and intrinsic network hub organization. Together, these results identify two principal neurochemical–network axes constraining shared and substance-specific cortical alteration patterns in SUD.

a. Permutation testing of significant LVs

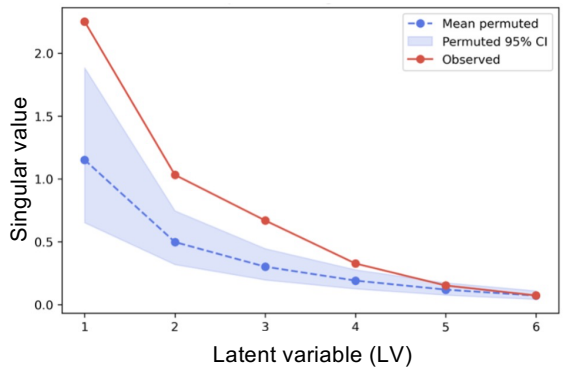

b. Percentage covariance explained

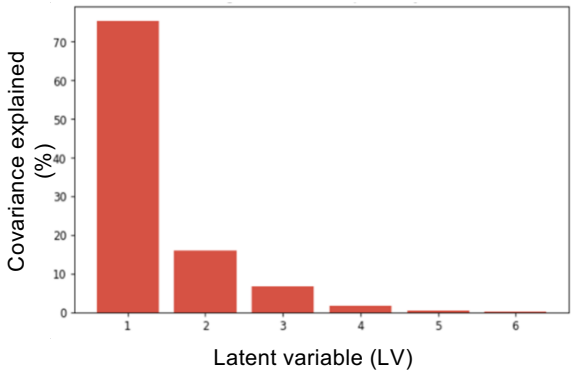

c. Projection of LV1-LV2 on brain surface

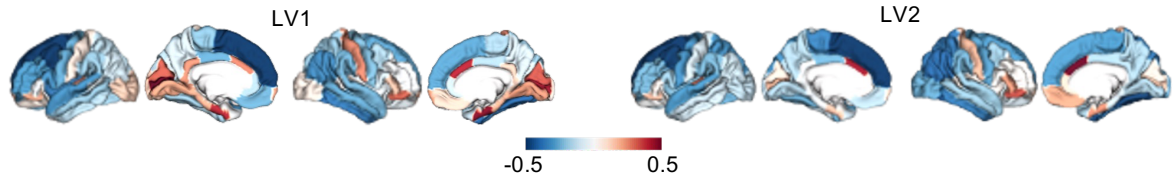

d. Loadings of LV1-LV2

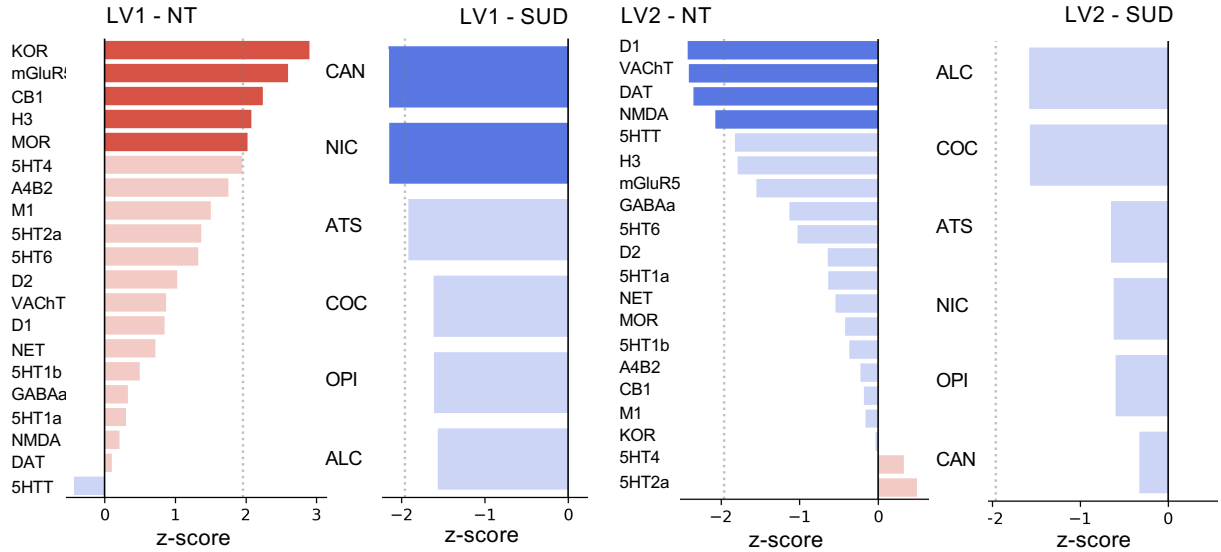

e. Hub vulnerability model for LV1-LV2

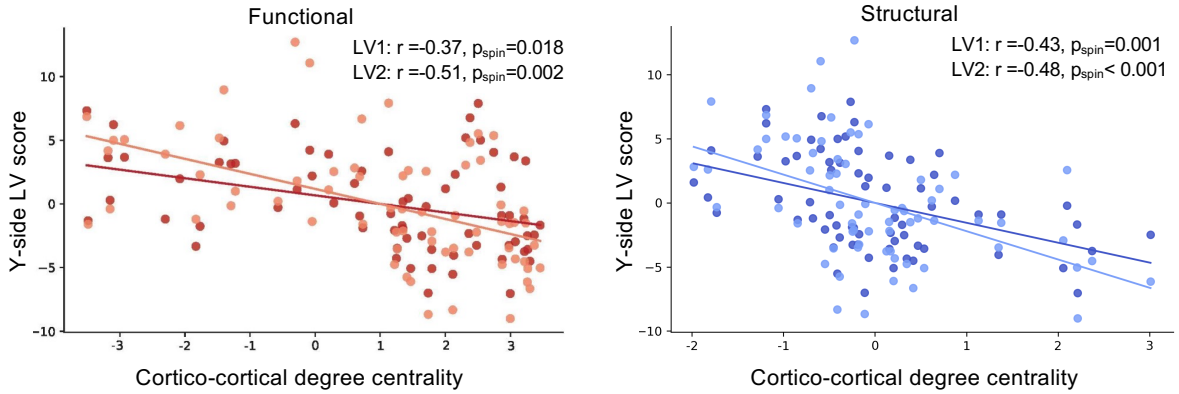

Fig. 6. Association of neurotransmitter density with cortical differences and epicenters in SUD. (a) Significance testing of partial least squares (PLS) latent variables (LVs) comparing observed singular values to a permutation-derived null distribution (mean ± 95% CI). Four LVs were significant. **(b)** Covariance explained by each LV, with LV1 and LV2 jointly accounting for ~90% of the total cross-covariance between standardized neurotransmitter receptor density and SUD-related cortical thickness differences. **(c)** Cortical maps of LV1 and LV2 scores, illustrating a shared frontotemporal vulnerability axis (LV1) and a secondary pattern with additional parietal involvement (LV2). Color scale reflects the loadings standardized between -0.5 and 0.5. **(d)** Permutation-based loading patterns for LV1–LV2. LV1 showed strong positive associations with cortical density of KOR, mGluR5, CB1, H3, and MOR receptors, and the largest negative SUD loadings for cannabis and nicotine. LV2 was characterized by negative loadings on D1, VAChT, DAT, and NMDA receptors and trend-level contributions from alcohol and cocaine. **(e)** Associations between LV scores and network centrality. Both LV1 and LV2 were negatively correlated with functional (FC) and structural (SC) centrality (all spin-test $p < 0.05$), indicating that neurotransmitter-related SUD axes preferentially involve highly connected cortical hubs.

Discussion

In this study, we characterized structural brain differences in individuals with substance use disorders (SUD), integrating large-scale structural MRI data with normative models of brain connectivity and molecular architecture. Across the six substance use disorders, we identified a reproducible, system-wide pattern of cortical and subcortical differences. These findings demonstrate involvement of frontal, parietal, and temporal association cortex and limbic subcortical structures, with the hippocampus and amygdala showing the largest volume reductions. Our findings align with previous results[8,51,52,80–82] and extend them by revealing broader regional involvement in SUD pathology. Significant SUD-by-age interactions indicated steeper age-related cortical thinning in SUD compared to controls, consistent with cumulative exposure–related effects and increased vulnerability to age-related brain changes. Across substances, we observed high spatial similarity, consistent with shared effects in distinct SUD[8,51,52]. Effect sizes were largest for alcohol and cocaine, differed across substances, and were robust to sample size differences. Overall, structural alterations in SUD were system-wide, graded across substances, and comparable in magnitude to those reported for schizophrenia and bipolar disorder[69–72].

In line with the hub vulnerability hypothesis[29,83], cortical morphometric differences in SUD were associated with functional and structural degree centrality, with greater alterations in highly connected hub regions. Cortical hubs are characterized by protracted developmental plasticity[58,84], dense neurotransmitter receptor

expression[44,45] and high metabolic demand[32,85]. They may therefore be particularly vulnerable to excitotoxicity, oxidative stress, and inflammatory processes[86], especially in chronic substance exposure[87,88]. Chronic stimulation of receptor systems concentrated in the association cortices may, through converging molecular pathways, contribute to the observed lower cortical thickness and age-dependent effects in hub regions.

We observed shared and substance-specific hub vulnerability patterns, with alcohol and cocaine showing stronger associations with functional hubs, whereas cannabis and nicotine showed relatively stronger associations with structural hubs. This divergence may reflect differences between functional connectivity, capturing transient co-activation, and structural connectivity, reflecting more stable anatomical pathways[30,89]. Such differences may begin to explain why certain substances preferentially affect functional coupling, whereas others alter structural integrity[13,86]. Future studies are necessary to clarify whether these differences are driven by substance-specific pharmacodynamic properties or heterogeneity in substance-use patterns.

Beyond hub vulnerability, epicenter mapping identified regions whose normative connectivity profiles matched the spatial distribution of SUD-related morphometric alterations, with functional epicenters distributed across associative networks and structural epicenters more confined to unimodal and sensorimotor territories. This suggests that SUD-related alterations may arise from multiple spatial "seeds" rather than a single focal point, consistent with parallel involvement of multiple neural circuits during chronic substance exposure[21,35,36]. Multiple epicenters may reflect combined distributed substance-related neurotoxic effects and neuroadaptation[21,35,90], as well as pre-existing network vulnerabilities[30,91], rather than a single cascade. Compared to other neuropsychiatric disorders[25,28], epicenters in SUD appeared more diffuse, potentially reflecting cumulative effects of substance exposure, including neuroadaptation as well as broader brain health processes such as neuroinflammation and cardiovascular burden[22,92–95]. In a transdiagnostic context, SUD epicenters overlapped substantially with those of schizophrenia and bipolar disorder[26], particularly within salience and frontoparietal control networks[96,97]. Structural epicenter overlap was more restricted but localized to inferior parietal cortex and inferior frontal gyrus (pars opercularis), key nodes of frontoparietal control and salience/inhibitory networks[98]. These networks support interoception, attention, cognitive control and salience attribution[97,99], functions affected across SUD, schizophrenia and bipolar disorder and potentially representing shared mechanisms of vulnerability[100]. Although schizophrenia and bipolar cohorts show high rates of nicotine dependence and comorbid SUD[101–105], this concern is mitigated by exclusion of major psychiatric disorders in our SUD cohorts and of current non-nicotine SUD in most schizophrenia and bipolar neuroimaging studies[69–72].

Our multivariate neurotransmitter mapping indicated that SUD-related morphometric differences align along two principal axes of neurotransmitter architecture. The dominant latent variable (LV1) loaded on κ-opioid, μ-

opioid, mGluR5, CB1, and H3 receptors and captured the cortical signature of the combined SUD phenotype, particularly in frontotemporal association cortices corresponding to hubs and epicenters. This is consistent with prior work showing that transmodal association cortex and hub-like regions are enriched in multiple receptor classes and anchor cross-disorder vulnerability gradients[45,106–109]. A second weaker latent variable (LV2) showed greater parietal involvement, particularly in alcohol- and cocaine-related profiles, and was associated with lower normative densities of D1, DAT, VAChT, and NMDA. This axis may reflect secondary vulnerability of regions with relatively sparse neuromodulatory input, potentially conferring reduced resilience to widespread neurochemical perturbations[110–112]. Dopamine and glutamate signaling are implicated in neurotrophic and spine-stabilizing processes[113–117], and disruptions during chronic substance use have been linked to synaptic and dendritic alterations in association circuits[4,118–120].

At the mechanistic level, these associations should be interpreted cautiously. The observed spatial correspondence between normative receptor distributions and SUD-related morphometric differences does not allow causal inference. It remains unclear whether regional receptor density predisposes areas to structural change, whether morphometric alterations secondarily affect receptor expression, or whether both reflect shared principles of network organization and chemoarchitecture[106,121]. Identifying causal pathways will require longitudinal designs combined with receptor- and circuit-level manipulations.

Our study has limitations. Although this represents the largest SUD neuroimaging cohort to date, sample sizes for opioids and amphetamine-type stimulants were modest and findings for these groups should be interpreted cautiously. Clinical heterogeneity and polysubstance use may have obscured morphometric brain differences unique to each substance. The cross-sectional design precludes inference about causality or temporal dynamics, and does not allow us to account for variation in substance exposure trajectories, including varying levels of consumption or abstinence patterns. In particular, cross-sectional data cannot disentangle temporary neuroplastic adaptations from longer-lasting neurotoxic effects. Longitudinal MRI studies demonstrate partial structural recovery with decreased consumption or abstinence[17,19], while animal models show that neurodegeneration and regeneration can co-occur, as a function of intake and abstinence duration[122,123]. Finally, the receptor and connectivity analyses relied on normative PET and connectome data that do not capture substance or disease-specific alterations.

In sum, brain alterations in SUD are shaped by large-scale network organization and neurotransmitter receptor architecture, rather than focal regional abnormalities. Across six distinct SUD we identified a largely shared pattern of cortical and subcortical morphometric differences with accelerated age-related effects. These findings suggest that normative connectivity and chemoarchitecture constitute organizing constraints shaping SUD-related brain pathology. Cross-disorder comparisons highlight shared structural substrates and potential

vulnerability mechanisms with schizophrenia and bipolar disorder. Together, this work provides a systems-level framework for understanding brain vulnerability in addiction and highlights receptor- and circuit-informed targets for prevention and intervention.

Methods

The overall analytic workflow, including data integration, morphometric modeling, and network-based analyses, is summarized in **Fig. 1**. All network-level modeling was conducted with Python version 3.10.13 using the open-source ENIGMA Toolbox[124]. Additional statistical analyses were carried out in R version 4.3.0.

ENIGMA Participants

We analyzed structural neuroimaging data from 2,782 individuals with substance use disorder (SUD; mean age = 34.6 ± 11.2 years; range: 18–67; 33.3% female, *n* = 926) and 1,951 healthy controls (mean age = 33.8 ± 12.0 years; range: 18–75; 37.5% female, *n* = 731) collected from 51 international sites contributing to the ENIGMA Addiction Working Group (Supplementary **Table S1**; **Fig. S1**). Participants with SUD met diagnostic criteria for one or more of six primary categories: alcohol, amphetamines, cannabis, cocaine, nicotine, and opioids. 2,312 individuals (mean age = 34.7 ± 11.3 years; range: 18–67; 33.9% female, *n* = 783) met criteria for a single SUD diagnosis without comorbidity of another SUD and were included in substance-specific analyses (alcohol: 902; amphetamines: 178; cannabis: 286; cocaine: 278; nicotine: 600; opioids: 68). Diagnoses were confirmed at each site using DSM-IV or ICD-10 criteria. Site-level demographic details are reported in Supplementary **Table S2**. Individuals were excluded if they had a lifetime history of neurological disease, a current DSM-IV/DSM-5 axis I diagnosis other than depressive and anxiety disorders, or any contraindication for MRI. Control subjects may have used addictive substances recreationally but were never diagnosed with any SUD. All studies were approved by local institutional review boards, and all participants provided written informed consent.

Primary analyses focused on the combined SUD (*n* = 2,782) and control sample (*n* = 1,951), which included all six substance categories, in line with prior ENIGMA work[8]. We then conducted substance-specific analyses, excluding individuals with more than one SUD, as secondary analyses (total *n* across substances = 2,312) to test the consistency of main findings across the individual SUD categories (see *Substance-specific Network Modeling and cross-correlation structure* of the Methods section).

Image acquisition and processing

High-resolution 3D volumetric T1-weighted structural brain MRI scans were acquired at each site using local acquisition protocols (for details, see Supplementary **Table S3** and Supplementary Methods). Imaging data were processed using the ENIGMA standard structural MRI pipeline with FreeSurfer version 5.3[46,47]. Cortical thickness was extracted from 68 bilateral regions using the Desikan–Killiany atlas[48]. Volumetric measures were obtained for 14 subcortical gray matter regions, including bilateral amygdala, thalamus, caudate, putamen, pallidum, nucleus accumbens, and bilateral hippocampi. All sites adhered to ENIGMA's standardized quality control procedures (http://enigma.usc.edu/protocols/imaging-protocols).

Statistical mega-analysis

To assess morphometric differences in cortical thickness (CT) and subcortical volume (SV) between individuals with SUD and healthy controls, we applied mega-analytical linear models across all 68 cortical and 14 subcortical regions. Morphometric data were harmonized across the 51 sites using ComBat, an empirical Bayes-based method for correcting batch effects[49,50]. After harmonization, linear models were fit using the *lm* function in R to compare the average morphometric difference profiles for CT and SV in the combined sample of patients with SUD (n = 2,782) relative to controls (n = 1,951), correcting for age, sex, and intracranial volume (ICV) for both cortical and subcortical measures, similar to previous work[8], to ensure comparability. In our substance-specific analysis subset (n = 2,312), groups of individuals with single SUD (alcohol: 902; amphetamines: 178; cannabis: 286; cocaine: 278; nicotine: 600; opioids: 68) were compared to controls (n = 1,951), applying the same linear model parameters. In a separate robustness analysis, an age-squared term was included as an additional covariate. Findings were corrected for multiple comparisons using the false discovery rate (FDR) procedure[125] (Supplementary **Tables S4–S5**). To assess the robustness of cortical thickness and subcortical volume alterations across substance use disorder categories, we implemented a leave-one-out (LOO) analysis by iteratively excluding each substance category. For each iteration, linear models were re-fit adjusting for age, sex, and intracranial volume. Region-wise leave-one-out Cohen's d maps are reported in Supplementary **Tables S6–S7**, whereas spatial similarity analyses for these cortical and subcortical alterations are provided in Supplementary **Tables S8–S9**.

Principal component analysis of substance-specific maps

To assess the shared variance structure across substance-specific morphometric differences, we performed a principal component analysis (PCA) on the region-wise effect-size maps (Cohen's d) for the six primary SUD groups (alcohol, amphetamines, cannabis, cocaine, nicotine, opioids). Separate PCA models were run for cortical thickness (68 regions) and subcortical volume (14 regions). For each modality, we constructed a region

× substance matrix containing the harmonized, covariate-adjusted effect sizes from the substance-specific case–control analyses. Effect-size vectors were mean-centered across substances, and PCA was performed using singular value decomposition. The first principal component (PC1) was retained as the dominant axis of shared morphometric variation and its loadings were projected onto cortical and subcortical surfaces for visualization. Spatial correspondence between PC1 and the combined SUD morphometric map was assessed using Pearson correlation.

Functional and structural connectivity matrix generation from HCP data

Normative functional and structural connectivity matrices were obtained from the ENIGMA Toolbox[124], based on resting-state fMRI and diffusion MRI data from 207 unrelated healthy young adults (83 males; mean age ± SD = 28.7 ± 3.7 years) from the Human Connectome Project (HCP). These data were preprocessed using the HCP minimal processing pipeline[54,55]. The derivation of the matrices is described in detail in the ENIGMA Toolbox documentation[124]. Briefly, functional and structural connectivity were parcellated into 68 cortical regions using the Desikan–Killiany atlas. Normative functional connectivity matrices were generated by computing pairwise correlations between the time series of all brain regions; negative connections were set to zero, otherwise functional connectivity matrices are unthresholded. For structural connectivity, reconstructed streamlines, weighted by the cross-section multipliers, were mapped onto the 68 cortical and 14 subcortical regions. These methods yield two pairs of 68 × 68 cortical and 14 × 68 subcortical matrices, representing functional and structural connectivity. Based on these, we computed functional and structural cortico-cortical and subcortico-cortical centrality for each region. Formally, in a network (here represented by the connectivity matrices), for node *i*, weighted degree centrality *kw* for each node is defined as:

$$k_i^w = \sum_{j \in N} W_{ij}$$

where N is the set of all nodes in the network, and W_{ij} represents the weight of the connection between nodes i and j. Thus, for each brain region, weighted cortico-cortical and subcortico-cortical degree centrality was calculated as the sum of the weights of all connections to other regions, excluding self-connections[126].

Hub vulnerability model

We tested the hub vulnerability hypothesis, which posits that more highly connected (central) brain regions are more susceptible to morphometric alteration in SUD[30–33]. We correlated the normative functional and structural centrality maps derived from cortico-cortical and subcortico-cortical connectivity with the regional CT and SV alterations, respectively. Centrality was defined as weighted degree centrality, reflecting the total strength of

functional or structural connections of each region, weighted by their respective magnitude[30,126]. Unthresholded centrality maps were used to avoid arbitrary cut-offs. To correct for spatial autocorrelation, significance was assessed using 10,000 surface-based spin permutations for cortical data[56,124,127]. For subcortical regions, a similar procedure was applied, but instead of projecting subcortical labels onto spheres as in the spin test, the labels were randomly shuffled[121] (Supplementary **Tables S10–S11**). As a robustness check, we replicated the analyses using numerous centrality measures, including strength, eigenvector, betweenness, and closeness centrality, which capture complementary aspects of nodal importance in the network. Detailed results of centrality–atrophy associations, as well as cross-metric consistency of hub vulnerability effects, are summarized in Supplementary **Tables S12–S13**.

Mapping disease epicenters

Epicenters were identified by correlating each region's normative connectivity profile (i.e., each row in the functional or structural connectivity matrix, represented as a vector) with the vector of SUD-related morphometric alterations[25,28,124]. Spatial autocorrelation was addressed using spin permutation tests (10,000 repetitions) for cortical regions and label shuffling (10,000 repetitions) for subcortical regions (Supplementary **Tables S14–S15**)[26,91,124].

Regions were considered epicenters if their correlation survived FDR correction ($p < 0.05$; $n = 68$ cortical, $n = 14$ subcortical structures). Please note that unlike hubs, epicenters need not exhibit structural alteration or high centrality but are defined by the alignment of their connectivity profiles with disease topography[26,28,85,128].

Substance-specific network modeling and cross-correlation structure

To examine whether our findings from the pooled sample of individuals with SUD are driven by specific substance subgroups or are shared across the six substance use disorders, we re-ran the linear models to compare cortical thickness and subcortical volume for each substance separately (Supplementary **Tables S4–S5**). We restricted these substance-specific analyses to cases with only one primary SUD, to increase specificity, and compared them with the pooled control sample (n = 1,951), to increase comparability of effects between substances. To ensure the robustness of the substance-specific findings to the latter methodological choices, we estimated morphometric differences in individuals with comorbid SUD (in addition to the primary diagnosis) and compared them to a non-pooled control sample (**Fig. S9**). Based on the substance-specific morphometric maps, we then tested the hub vulnerability model (Supplementary **Tables S10–S13**) and performed functional and structural epicenter mapping (Supplementary **Tables S14–S15**), correcting for spatial autocorrelation and multiple testing (FDR). We next assessed the spatial similarity between the combined SUD

epicenter map and the six individual substance epicenter maps, and computed cross-substance spatial correlations for all pairs (Supplementary **Tables S16–S17**). We also identified epicenters that were unique to a given substance or shared across multiple substances, by superimposing the brain maps, restricting analyses to regions that survived spin-test correction ($p_{spin} < 0.05$) in substance-specific maps (Supplementary **Tables S18–S19**).

Robustness and generalizability analyses

Age and sex interaction analysis

To examine demographic moderators, we modelled age and sex effects on CT and SV in the combined SUD phenotype. SUD-by-age and SUD-by-sex interaction models were fit to identify regions where moderator variable effects interacted with SUD-related effects. If a widespread and spatially consistent pattern of significant interactions was observed across cortical regions (FDR-p_{spin} < 0.05) for the interaction terms (diagnosis*sex or diagnosis*age), we subsequently tested the hub vulnerability and epicenter models using the resulting interaction effect maps (Supplementary **Tables S20–S24**).

Subject-level cortical abnormality modeling

To evaluate whether network-based markers of cortical vulnerability extend to the individual level, we computed subject-specific cortical thickness (CT) abnormality maps in participants with SUD. For each individual, CT values were residualized for age and sex and then z-scored relative to the healthy control (HC) distribution. These individualized z-score maps were spatially correlated with normative functional and structural degree centrality maps to derive hub vulnerability scores. To identify epicenters, we assessed for each cortical region whether its normative connectivity profile significantly aligned with the participant's z-score map using spin-based spatial permutation testing ($p_{spin} < 0.05$). Aggregated epicenter maps were generated by calculating, for each region, the proportion of individuals in whom that region was identified as an epicenter. Significant differences of proportions in hub vulnerability and epicenter frequency at the individual level were evaluated using chi-square tests (Supplementary **Table S25**).

Robustness of SUD-specific morphometric differences to age distribution

To assess whether differences in case–control effect size magnitudes across SUD subgroups, particularly the larger effects observed for alcohol and cocaine, could be attributable to age-distribution imbalances, we conducted an age harmonization bootstrap analysis. An anchor reference age was defined using the rest of the subgroups (amphetamines/cannabis/nicotine/opioids), from which we computed the anchor mean age. For each

subgroup we resampled a fixed fraction of available cases (60%) without replacement across bootstrap iterations. For alcohol and cocaine, we applied weighted rejection sampling to preferentially select younger participants: candidate samples were drawn without replacement using age-dependent weights (exponential decay of inclusion probability with increasing age), and were accepted only if the achieved mean age fell within ±2 years of the target mean age. For all other substances, cases were sampled uniformly from the subgroup (preserving each subgroup's natural age distribution). Within each accepted bootstrap iteration, controls were sampled without replacement to match the age composition of the corresponding case sample using age-bin count matching (fixed-width bins), yielding age-aligned case–control samples. Brain morphometric case–control differences were then estimated separately for cortical and subcortical metrics using linear models adjusted for age, sex, and ICV. The case–control contrast was converted to Cohen's *d* and summarized per iteration by the median effect across regions (Supplementary **Tables S26–S27**).

Robustness of median SUD-specific morphometric differences to sample size

To evaluate whether the observed differences in case–control effect sizes across substance-use subgroups were driven by unequal sample sizes rather than true underlying neuroanatomical variation, we performed a controlled bootstrap resampling analysis with equalized sample sizes. For each SUD group, we repeatedly resampled cases and matched controls with replacement to a fixed equalized sample size, and recomputed region-wise case–control Cohen's *d* values. This procedure was repeated across a sequence of target sample sizes (range = 25–300), with 500 bootstrap iterations per setting. For each substance and each sample size, effect distributions were summarized by the median Cohen's *d* across all cortical and, separately, subcortical regions, together with median 95% bootstrap confidence interval width. Substances with smaller original cohort sizes (e.g., opioids, amphetamines) were included in the larger-n conditions by sampling with replacement (upsampling), so that all groups were evaluated under the same controlled sample-size grid.

Robustness of SUD-specific morphometric difference between regional patterns to sample size

To assess how sample size influences the stability of regional morphometric difference patterns, we examined the spatial correspondence between bootstrap-derived regional effect-size maps and a high-n reference pattern, rather than focusing on absolute effect magnitudes. For each substance and each target sample size (n = 25–300), we repeatedly resampled n cases and n matched controls with replacement and recomputed the full vector of region-wise Cohen's *d* values.

Each bootstrap-derived effect-size vector was then correlated (Pearson r) with the Cohen's *d* pattern derived from the largest available permutation sample (n = 300), yielding a distribution of spatial correlation values per

substance and sample size. This procedure was repeated for 500 bootstrap iterations at each *n*. For each substance and *n*, we summarized spatial stability by the median correlation and its 95% bootstrap confidence interval, as well as the standard deviation across iterations. Substances with smaller original samples were upsampled with replacement to allow evaluation across the full sample-size range.

Robustness of SUD-specific brain morphometric differences to control samples

To assess whether substance-specific morphometric differences were influenced by the size or composition of the healthy control sample, we repeated all case–control analyses using three alternative control-sampling strategies. Method 1 (primary analysis) compared each single-SUD group (**Fig. 2a**; Supplementary **Table S2**; *Case SUD n*: alcohol: 902; amphetamines: 178; cannabis: 286; cocaine: 278; nicotine: 600; opioids: 68) to the full pooled healthy control group (*n* = 1,951). For the robustness analyses, we used non-pooled, study-specific healthy control samples (control *n*; alcohol: 765, amphetamines: 233, cannabis: 247, cocaine: 291, nicotine: 327, opioids: 88) and recomputed effect sizes using two comparison strategies. First, similar to the methodology of the primary (pooled) analysis, we compared each substance-specific control group to individuals with a single, non-comorbid SUD diagnosis (Supplementary **Table S2**; *Case SUD n*: alcohol: 902; amphetamines: 178; cannabis: 286; cocaine: 278; nicotine: 600; opioids: 68). Second, we compared the same substance-specific control group to individuals with at least one comorbid SUD diagnosis (Supplementary **Table S2**; *Case and comorbid SUD n*: alcohol: 1216; amphetamines: 185; cannabis: 288; cocaine: 404; nicotine: 662; opioids: 92). For each method, region-wise Cohen's *d* values were recomputed using the same covariate-adjusted linear models as in the main analysis. Spatial correspondence between effect-size maps derived from different control samples was quantified using Pearson correlations (Fig. S9), allowing direct evaluation of the influence of control-sample size and composition on the stability of substance-specific morphometric patterns (Supplementary **Tables S28–S30**).

Transdiagnostic disorder comparison

We used meta-analytical structural brain maps from the ENIGMA consortium for schizophrenia[69,70], bipolar disorder[71,72], major depressive disorder[73,74], obsessive-compulsive disorder[75,76], attention-deficit/hyperactivity disorder[77,78], and autism spectrum disorder[79]. For each disorder, functional and structural epicenters were computed using the same mapping procedure as our SUD analysis (Supplementary **Tables S31–S34**).

These were then compared with SUD epicenter maps to calculate cross-disorder spatial similarity (**Fig. 5a**; Supplementary **Tables S35–S36**), with significance determined using spin tests and FDR correction. Only

regions identified as significant epicenters in both SUD and each of the disorders were included in the overlap analyses (Supplementary **Tables S37–S38**).

Association of neurotransmitter density with cortical alterations and the connectome in SUD

We analyzed 20 PET-derived cortical receptor maps spanning serotonergic, dopaminergic, cholinergic, glutamatergic, GABAergic, cannabinoid, and opioid systems, aligned to the Desikan–Killiany atlas (68 regions; full list in Supplementary **Table S39)** derived from previously published PET datasets[45] and original receptor-specific PET studies. All receptor maps were z-scored across regions and assembled into a neurotransmitter matrix. Data can be obtained here: https://github.com/netneurolab/hansen_crossdisorder_vulnerability.git, and https://github.com/netneurolab/hansen_receptors.git.

SUD-related cortical alterations were quantified as regional Cohen's *d* effect sizes for each of the six substance groups. These maps were also z-scored and organized into a second matrix representing SUD effects across the same 68 cortical regions.

To identify shared spatial structure between neurotransmitter distributions and SUD-related cortical differences, we used partial least squares (PLS) analysis. This multivariate approach identifies pairs of latent variables (LVs) that maximize the covariance between the neurotransmitter and SUD matrices. The analysis yields (*i*) loading patterns for each neurotransmitter receptor and each SUD map, and (*ii*) region-wise LV scores that capture the spatial expression of each multivariate pattern.

To assess statistical significance, we performed 10,000 permutation tests in which the spatial order of the SUD matrix was randomly shuffled while the neurotransmitter matrix was kept intact. For each permutation, the full PLS solution was recomputed, generating a null distribution against which the observed latent variables were evaluated. We considered an LV significant if its associated singular value exceeded the 95% range of the permutation distribution. To evaluate the robustness of individual neurotransmitter and SUD loadings, we additionally computed permutation-based loading ratios by comparing observed loadings to the variability of loadings across permutations.

We next examined whether the spatial expression of significant LVs reflected underlying network constraints. For this purpose, we used functional and structural connectomes from the ENIGMA Toolbox[124] (fsaverage5; Desikan–Killiany parcellation) and computed degree centrality for each cortical region. Correlations between LV scores and centrality were performed separately for functional and structural networks. Because cortical maps exhibit strong spatial autocorrelation, all correlations were evaluated using spin spatial permutation testing (10,000 repetitions)[56].

Data availability

All data reported in the manuscript are included in the article and its supplementary information files. Summary statistics of the case-control meta-analyses from the ENIGMA Working Groups are available from the ENIGMA Toolbox (https://enigma-toolbox.readthedocs.io/en/latest/). Preprocessed normative cortico-cortical, subcortico-cortical, and subcortico-subcortical functional and structural connectivity data are available from the ENIGMA Toolbox (https://enigma-toolbox.readthedocs.io/en/latest/). Molecular, connectivity, and receptor datasets are available from https://github.com/netneurolab/hansen_crossdisorder_vulnerability.git and https://github.com/netneurolab/hansen_receptors.git. Additional information can be made available upon reasonable request to the authors.

Code availability

All software and analysis code used in this study are openly available. Image preprocessing pipelines are available through the ENIGMA consortium (https://github.com/ENIGMA-git). The network modeling code is publicly available from the ENIGMA toolbox https://enigma-toolbox.readthedocs.io/en/latest/[124]. All further statistical analyses were performed in R version 4.3.0. The respective packages are mentioned in the corresponding "Methods" sections.

Competing interests

MK has received consulting fees from Otsuka for activities unrelated to the present study. All other authors declare that they have no conflicts of interest related to this study.

Funding

Core funding for ENIGMA was provided by the NIH Big Data to Knowledge (BD2K) program under consortium grant U54 EB020403 (PI: PMT). FG was supported by a research grant (230273) from the Hans and Marianne Schwyn Foundation; BAM was supported by Santa Anna Scuola Superiore Universitaria Pisa (SFS); SLV was supported by the Max Planck Society; the Helmholtz International BigBrain Analytics and Learning Laboratory (Hiball); Jacobs foundation research fellowship and Hector foundation research development award. MK acknowledges funding from the Swiss National Science Foundation (P2SKP3_178175 and grant number 32003B_219240).

References

1. The United Nations Office on Drugs and Crime (UNODC). World Drug Report. in (https://www.unodc.org/unodc/en/data-and-analysis/wdr2023_annex.html).
2. GBD 2016 Alcohol and Drug Use Collaborators. The global burden of disease attributable to alcohol and drug use in 195 countries and territories, 1990-2016: a systematic analysis for the Global Burden of Disease Study 2016. *Lancet Psychiatry* **5**, 987–1012 (2018).
3. Stone, A. L., Becker, L. G., Huber, A. M. & Catalano, R. F. Review of risk and protective factors of substance use and problem use in emerging adulthood. *Addict Behav* **37**, 747–775 (2012).
4. Hawkins, J. D., Catalano, R. F. & Miller, J. Y. Risk and protective factors for alcohol and other drug problems in adolescence and early adulthood: implications for substance abuse prevention. *Psychol Bull* **112**, 64–105 (1992).
5. Goldstein, R. Z. & Volkow, N. D. Dysfunction of the prefrontal cortex in addiction: neuroimaging findings and clinical implications. *Nat Rev Neurosci* **12**, 652–669 (2011).
6. Volkow, N. D., Michaelides, M. & Baler, R. The Neuroscience of Drug Reward and Addiction. *Physiol Rev* **99**, 2115–2140 (2019).
7. Joutsa, J. *et al.* Brain lesions disrupting addiction map to a common human brain circuit. *Nat Med* **28**, 1249–1255 (2022).
8. Mackey, S. *et al.* Mega-Analysis of Gray Matter Volume in Substance Dependence: General and Substance-Specific Regional Effects. *Am J Psychiatry* **176**, 119–128 (2019).
9. Cao, Z. *et al.* Mapping cortical and subcortical asymmetries in substance dependence: Findings from the ENIGMA Addiction Working Group. *Addict Biol* **26**, e13010 (2021).
10. Tolomeo, S. & Yu, R. Brain network dysfunctions in addiction: a meta-analysis of resting-state functional connectivity. *Transl Psychiatry* **12**, 41 (2022).
11. Taebi, A. *et al.* Shared network-level functional alterations across substance use disorders: A multi-level kernel density meta-analysis of resting-state functional connectivity studies. *Addict Biol* **27**, e13200 (2022).
12. Daviet, R. *et al.* Associations between alcohol consumption and gray and white matter volumes in the UK Biobank. *Nat Commun* **13**, 1175 (2022).
13. Ottino-González, J. *et al.* White matter microstructure differences in individuals with dependence on cocaine, methamphetamine, and nicotine: Findings from the ENIGMA-Addiction working group. *Drug Alcohol Depend* **230**, 109185 (2022).
14. Topiwala, A. *et al.* Associations between moderate alcohol consumption, brain iron, and cognition in UK Biobank participants: Observational and mendelian randomization analyses. *PLoS Med* **19**, e1004039 (2022).
15. Thompson, P. M. *et al.* ENIGMA and global neuroscience: A decade of large-scale studies of the brain in health and disease across more than 40 countries. *Transl Psychiatry* **10**, 100 (2020).
16. Scheffler, F. *et al.* Mega-analysis of the brain-age gap in substance use disorder: An ENIGMA Addiction working group study. *Addiction* **119**, 1937–1946 (2024).
17. Hirsiger, S. *et al.* Longitudinal changes in cocaine intake and cognition are linked to cortical thickness adaptations in cocaine users. *Neuroimage Clin* **21**, 101652 (2019).
18. Meier, M. H. *et al.* Long-Term Cannabis Use and Cognitive Reserves and Hippocampal Volume in Midlife. *Am J Psychiatry* **179**, 362–374 (2022).
19. Gaudreault, P.-O. *et al.* Frontal White Matter Changes and Craving Recovery in Inpatients With Heroin Use Disorder. *JAMA Netw Open* **7**, e2451678 (2024).
20. Tolomeo, S., Gray, S., Matthews, K., Steele, J. D. & Baldacchino, A. Multifaceted impairments in impulsivity and brain structural abnormalities in opioid dependence and abstinence. *Psychol Med* **46**, 2841–2853 (2016).

21. Cadet, J. L., Bisagno, V. & Milroy, C. M. Neuropathology of substance use disorders. *Acta Neuropathol* **127**, 91–107 (2014).
22. Lacagnina, M. J., Rivera, P. D. & Bilbo, S. D. Glial and Neuroimmune Mechanisms as Critical Modulators of Drug Use and Abuse. *Neuropsychopharmacology* **42**, 156–177 (2017).
23. Zahr, N. M., Kaufman, K. L. & Harper, C. G. Clinical and pathological features of alcohol-related brain damage. *Nat Rev Neurol* **7**, 284–294 (2011).
24. Gerring, Z. F., Thorp, J. G., Treur, J. L., Verweij, K. J. H. & Derks, E. M. The genetic landscape of substance use disorders. *Mol Psychiatry* **29**, 3694–3705 (2024).
25. Hettwer, M. D. *et al.* Coordinated cortical thickness alterations across six neurodevelopmental and psychiatric disorders. *Nat Commun* **13**, 6851 (2022).
26. Georgiadis, F. *et al.* Connectome architecture shapes large-scale cortical alterations in schizophrenia: a worldwide ENIGMA study. *Mol Psychiatry* **29**, 1869–1881 (2024).
27. Shafiei, G. *et al.* Spatial Patterning of Tissue Volume Loss in Schizophrenia Reflects Brain Network Architecture. *Biol Psychiatry* **87**, 727–735 (2020).
28. Larivière, S. *et al.* Network-based atrophy modeling in the common epilepsies: A worldwide ENIGMA study. *Sci. Adv.* **6**, eabc6457 (2020).
29. Crossley, N. A. *et al.* The hubs of the human connectome are generally implicated in the anatomy of brain disorders. *Brain* **137**, 2382–2395 (2014).
30. Fornito, A., Zalesky, A. & Breakspear, M. The connectomics of brain disorders. *Nat Rev Neurosci* **16**, 159–172 (2015).
31. Power, J. D., Schlaggar, B. L., Lessov-Schlaggar, C. N. & Petersen, S. E. Evidence for hubs in human functional brain networks. *Neuron* **79**, 798–813 (2013).
32. van den Heuvel, M. P. & Sporns, O. Network hubs in the human brain. *Trends Cogn Sci* **17**, 683–696 (2013).
33. Van Den Heuvel, M. P. & Seoane, S. L. Support for network theories of schizophrenia. *Nat Rev Neurol* **20**, 381–382 (2024).
34. Buckner, R. L. *et al.* Cortical hubs revealed by intrinsic functional connectivity: mapping, assessment of stability, and relation to Alzheimer's disease. *J Neurosci* **29**, 1860–1873 (2009).
35. Volkow, N. D. & Morales, M. The Brain on Drugs: From Reward to Addiction. *Cell* **162**, 712–725 (2015).
36. Everitt, B. J. & Robbins, T. W. Drug Addiction: Updating Actions to Habits to Compulsions Ten Years On. *Annu Rev Psychol* **67**, 23–50 (2016).
37. Zhou, J., Gennatas, E. D., Kramer, J. H., Miller, B. L. & Seeley, W. W. Predicting regional neurodegeneration from the healthy brain functional connectome. *Neuron* **73**, 1216–1227 (2012).
38. Seeley, W. W., Crawford, R. K., Zhou, J., Miller, B. L. & Greicius, M. D. Neurodegenerative diseases target large-scale human brain networks. *Neuron* **62**, 42–52 (2009).
39. Zeighami, Y. *et al.* Network structure of brain atrophy in de novo Parkinson's disease. *Elife* **4**, e08440 (2015).
40. Zhou, J. & Seeley, W. W. Network dysfunction in Alzheimer's disease and frontotemporal dementia: implications for psychiatry. *Biol Psychiatry* **75**, 565–573 (2014).
41. Jiang, Y. *et al.* Neuroimaging epicenters as potential sites of onset of the neuroanatomical pathology in schizophrenia. *Sci Adv* **10**, eadk6063 (2024).
42. Chopra, S. *et al.* Network-Based Spreading of Gray Matter Changes Across Different Stages of Psychosis. *JAMA Psychiatry* **80**, 1246–1257 (2023).
43. Fan, Y.-S. *et al.* Neurodevelopmentally rooted epicenters in schizophrenia: sensorimotor-association spatial axis of cortical thickness alterations. *Mol Psychiatry* **31**, 929–940 (2026).
44. Zilles, K. & Amunts, K. Receptor mapping: architecture of the human cerebral cortex. *Curr Opin Neurol* **22**, 331–339 (2009).

45. Hansen, J. Y. *et al.* Mapping neurotransmitter systems to the structural and functional organization of the human neocortex. *Nat Neurosci* **25**, 1569–1581 (2022).
46. Fischl, B. FreeSurfer. *Neuroimage* **62**, 774–781 (2012).
47. Fischl, B. *et al.* Whole brain segmentation: automated labeling of neuroanatomical structures in the human brain. *Neuron* **33**, 341–355 (2002).
48. Desikan, R. S. *et al.* An automated labeling system for subdividing the human cerebral cortex on MRI scans into gyral based regions of interest. *Neuroimage* **31**, 968–980 (2006).
49. Leek, J. T., Johnson, W. E., Parker, H. S., Jaffe, A. E. & Storey, J. D. The sva package for removing batch effects and other unwanted variation in high-throughput experiments. *Bioinformatics* **28**, 882–883 (2012).
50. Fortin, J.-P. *et al.* Harmonization of cortical thickness measurements across scanners and sites. *Neuroimage* **167**, 104–120 (2018).
51. Hill-Bowen, L. D. *et al.* Convergent gray matter alterations across drugs of abuse and network-level implications: A meta-analysis of structural MRI studies. *Drug and Alcohol Dependence* **240**, 109625 (2022).
52. Chye, Y. *et al.* Subcortical surface morphometry in substance dependence: An ENIGMA addiction working group study. *Addiction Biology* **25**, e12830 (2020).
53. Ersche, K. D. *et al.* Brain networks underlying vulnerability and resilience to drug addiction. *Proc Natl Acad Sci U S A* **117**, 15253–15261 (2020).
54. Van Essen, D. C. *et al.* The Human Connectome Project: a data acquisition perspective. *Neuroimage* **62**, 2222–2231 (2012).
55. Glasser, M. F. *et al.* The minimal preprocessing pipelines for the Human Connectome Project. *Neuroimage* **80**, 105–124 (2013).
56. Alexander-Bloch, A. F. *et al.* On testing for spatial correspondence between maps of human brain structure and function. *Neuroimage* **178**, 540–551 (2018).
57. Dima, D. *et al.* Subcortical volumes across the lifespan: Data from 18,605 healthy individuals aged 3-90 years. *Hum Brain Mapp* **43**, 452–469 (2022).
58. Bethlehem R. A. I. *et al.* Brain charts for the human lifespan. *Nature* **604**, 525–533 (2022).
59. Frangou, S. *et al.* Cortical thickness across the lifespan: Data from 17,075 healthy individuals aged 3-90 years. *Hum Brain Mapp* **43**, 431–451 (2022).
60. Storsve, A. B. *et al.* Differential longitudinal changes in cortical thickness, surface area and volume across the adult life span: regions of accelerating and decelerating change. *J Neurosci* **34**, 8488–8498 (2014).
61. Ritchie, S. J. *et al.* Sex Differences in the Adult Human Brain: Evidence from 5216 UK Biobank Participants. *Cerebral Cortex* **28**, 2959–2975 (2018).
62. Lotze, M. *et al.* Novel findings from 2,838 Adult Brains on Sex Differences in Gray Matter Brain Volume. *Sci Rep* **9**, 1671 (2019).
63. Wierenga, L. M. *et al.* Greater male than female variability in regional brain structure across the lifespan. *Hum Brain Mapp* **43**, 470–499 (2022).
64. Schnack, H. G. *et al.* Accelerated Brain Aging in Schizophrenia: A Longitudinal Pattern Recognition Study. *Am J Psychiatry* **173**, 607–616 (2016).
65. Han, L. K. M. *et al.* Brain aging in major depressive disorder: results from the ENIGMA major depressive disorder working group. *Mol Psychiatry* **26**, 5124–5139 (2021).
66. Schinz, D. *et al.* Lower cortical thickness and increased brain aging in adults with cocaine use disorder. *Front. Psychiatry* **14**, 1266770 (2023).
67. Sun, D. *et al.* Adolescent alcohol use is linked to disruptions in age-appropriate cortical thinning: an unsupervised machine learning approach. *Neuropsychopharmacology* **48**, 317–326 (2023).

68. Navarri, X. *et al.* How do substance use disorders compare to other psychiatric conditions on structural brain abnormalities? A cross-disorder meta-analytic comparison using the ENIGMA consortium findings. *Hum Brain Mapp* **43**, 399–413 (2022).
69. van Erp, T. G. M. *et al.* Cortical Brain Abnormalities in 4474 Individuals With Schizophrenia and 5098 Control Subjects via the Enhancing Neuro Imaging Genetics Through Meta Analysis (ENIGMA) Consortium. *Biol Psychiatry* **84**, 644–654 (2018).
70. van Erp, T. G. M. *et al.* Subcortical brain volume abnormalities in 2028 individuals with schizophrenia and 2540 healthy controls via the ENIGMA consortium. *Mol Psychiatry* **21**, 547–553 (2016).
71. Hibar, D. P. *et al.* Cortical abnormalities in bipolar disorder: an MRI analysis of 6503 individuals from the ENIGMA Bipolar Disorder Working Group. *Mol Psychiatry* **23**, 932–942 (2018).
72. Hibar, D. P. *et al.* Subcortical volumetric abnormalities in bipolar disorder. *Mol Psychiatry* **21**, 1710–1716 (2016).
73. Schmaal, L. *et al.* Cortical abnormalities in adults and adolescents with major depression based on brain scans from 20 cohorts worldwide in the ENIGMA Major Depressive Disorder Working Group. *Mol Psychiatry* **22**, 900–909 (2017).
74. Schmaal, L. *et al.* Subcortical brain alterations in major depressive disorder: findings from the ENIGMA Major Depressive Disorder working group. *Mol Psychiatry* **21**, 806–812 (2016).
75. Boedhoe, P. S. W. *et al.* Cortical Abnormalities Associated With Pediatric and Adult Obsessive-Compulsive Disorder: Findings From the ENIGMA Obsessive-Compulsive Disorder Working Group. *Am J Psychiatry* **175**, 453–462 (2018).
76. Boedhoe, P. S. W. *et al.* Distinct Subcortical Volume Alterations in Pediatric and Adult OCD: A Worldwide Meta- and Mega-Analysis. *Am J Psychiatry* **174**, 60–69 (2017).
77. Hoogman, M. *et al.* Brain Imaging of the Cortex in ADHD: A Coordinated Analysis of Large-Scale Clinical and Population-Based Samples. *Am J Psychiatry* **176**, 531–542 (2019).
78. Hoogman, M. *et al.* Subcortical brain volume differences in participants with attention deficit hyperactivity disorder in children and adults: a cross-sectional mega-analysis. *Lancet Psychiatry* **4**, 310–319 (2017).
79. van Rooij, D. *et al.* Cortical and Subcortical Brain Morphometry Differences Between Patients With Autism Spectrum Disorder and Healthy Individuals Across the Lifespan: Results From the ENIGMA ASD Working Group. *Am J Psychiatry* **175**, 359–369 (2018).
80. Kühn, S. & Gallinat, J. Common biology of craving across legal and illegal drugs - a quantitative meta-analysis of cue-reactivity brain response. *Eur J Neurosci* **33**, 1318–1326 (2011).
81. Mackey, S. & Paulus, M. Are there volumetric brain differences associated with the use of cocaine and amphetamine-type stimulants? *Neurosci Biobehav Rev* **37**, 300–316 (2013).
82. Ersche, K. D. *et al.* Abnormal brain structure implicated in stimulant drug addiction. *Science* **335**, 601–604 (2012).
83. Buckholtz, J. W. & Meyer-Lindenberg, A. Psychopathology and the human connectome: toward a transdiagnostic model of risk for mental illness. *Neuron* **74**, 990–1004 (2012).
84. Sydnor, V. J. *et al.* Neurodevelopment of the association cortices: Patterns, mechanisms, and implications for psychopathology. *Neuron* **109**, 2820–2846 (2021).
85. van den Heuvel, M. P., Kahn, R. S., Goñi, J. & Sporns, O. High-cost, high-capacity backbone for global brain communication. *Proc Natl Acad Sci U S A* **109**, 11372–11377 (2012).
86. Koob, G. F. & Volkow, N. D. Neurobiology of addiction: a neurocircuitry analysis. *Lancet Psychiatry* **3**, 760–773 (2016).
87. Volkow, N. D., Koob, G. F. & McLellan, A. T. Neurobiologic Advances from the Brain Disease Model of Addiction. *N Engl J Med* **374**, 363–371 (2016).
88. Crews, F. T., Lawrimore, C. J., Walter, T. J. & Coleman, L. G. The role of neuroimmune signaling in alcoholism. *Neuropharmacology* **122**, 56–73 (2017).

89. Honey, C. J. *et al.* Predicting human resting-state functional connectivity from structural connectivity. *Proc Natl Acad Sci U S A* **106**, 2035–2040 (2009).
90. Büttner, A. Review: The neuropathology of drug abuse. *Neuropathol Appl Neurobiol* **37**, 118–134 (2011).
91. Alexander-Bloch, A., Giedd, J. N. & Bullmore, E. Imaging structural co-variance between human brain regions. *Nat Rev Neurosci* **14**, 322–336 (2013).
92. Morcuende, A., Navarrete, F., Nieto, E., Manzanares, J. & Femenía, T. Inflammatory Biomarkers in Addictive Disorders. *Biomolecules* **11**, 1824 (2021).
93. Kohno, M. *et al.* Neuroinflammation in addiction: A review of neuroimaging studies and potential immunotherapies. *Pharmacology Biochemistry and Behavior* **179**, 34–42 (2019).
94. Gan, W. Q. *et al.* Risk of cardiovascular diseases in relation to substance use disorders. *Drug Alcohol Depend* **229**, 109132 (2021).
95. Benowitz, N. L. & Liakoni, E. Tobacco use disorder and cardiovascular health. *Addiction* **117**, 1128–1138 (2022).
96. Seeley, W. W. *et al.* Dissociable intrinsic connectivity networks for salience processing and executive control. *J Neurosci* **27**, 2349–2356 (2007).
97. Menon, V. Large-scale brain networks and psychopathology: a unifying triple network model. *Trends Cogn Sci* **15**, 483–506 (2011).
98. Dosenbach, N. U. F., Fair, D. A., Cohen, A. L., Schlaggar, B. L. & Petersen, S. E. A dual-networks architecture of top-down control. *Trends Cogn Sci* **12**, 99–105 (2008).
99. Cole, M. W. & Schneider, W. The cognitive control network: Integrated cortical regions with dissociable functions. *Neuroimage* **37**, 343–360 (2007).
100. Grotzinger, A. D. *et al.* Mapping the genetic landscape across 14 psychiatric disorders. *Nature* **649**, 406–415 (2026).
101. Diaz, F. J. *et al.* Tobacco smoking behaviors in bipolar disorder: a comparison of the general population, schizophrenia, and major depression. *Bipolar Disord* **11**, 154–165 (2009).
102. Koster, M. *et al.* The Association Between Chronic Tobacco Smoking and Brain Alterations in Schizophrenia: A Systematic Review of Magnetic Resonance Imaging Studies. *Schizophr Bull* **51**, 608–624 (2025).
103. Hunt, G. E., Large, M. M., Cleary, M., Lai, H. M. X. & Saunders, J. B. Prevalence of comorbid substance use in schizophrenia spectrum disorders in community and clinical settings, 1990–2017: Systematic review and meta-analysis. *Drug and Alcohol Dependence* **191**, 234–258 (2018).
104. Jørgensen, K. N. *et al.* Cigarette smoking is associated with thinner cingulate and insular cortices in patients with severe mental illness. *J Psychiatry Neurosci* **40**, 241–249 (2015).
105. Grunze, H., Schaefer, M., Scherk, H., Born, C. & Preuss, U. W. Comorbid Bipolar and Alcohol Use Disorder-A Therapeutic Challenge. *Front Psychiatry* **12**, 660432 (2021).
106. Hansen, J. Y. *et al.* Local molecular and global connectomic contributions to cross-disorder cortical abnormalities. *Nat Commun* **13**, 4682 (2022).
107. Hänisch, B. *et al.* Cerebral chemoarchitecture shares organizational traits with brain structure and function. *Elife* **12**, e83843 (2023).
108. Hansen, J. Y. *et al.* Integrating multimodal and multiscale connectivity blueprints of the human cerebral cortex in health and disease. *PLoS Biol* **21**, e3002314 (2023).
109. Coray, R. C. *et al.* Memory deficits of MDMA users are linked to cortical thinning related to 5-HT receptor densities. *Brain* awaf391 (2025) doi:10.1093/brain/awaf391.
110. Volkow, N. D., Fowler, J. S., Wang, G. J., Baler, R. & Telang, F. Imaging dopamine's role in drug abuse and addiction. *Neuropharmacology* **56 Suppl 1**, 3–8 (2009).
111. Anderson, S. M. & Pierce, R. C. Cocaine-induced alterations in dopamine receptor signaling: implications for reinforcement and reinstatement. *Pharmacol Ther* **106**, 389–403 (2005).

112. Park, K., Volkow, N. D., Pan, Y. & Du, C. Chronic cocaine dampens dopamine signaling during cocaine intoxication and unbalances D1 over D2 receptor signaling. *J Neurosci* **33**, 15827–15836 (2013).
113. Wang, C. S., Kavalali, E. T. & Monteggia, L. M. BDNF signaling in context: From synaptic regulation to psychiatric disorders. *Cell* **185**, 62–76 (2022).
114. Chapleau, C. A., Carlo, M. E., Larimore, J. L. & Pozzo-Miller, L. The actions of BDNF on dendritic spine density and morphology in organotypic slice cultures depend on the presence of serum in culture media. *J Neurosci Methods* **169**, 182–190 (2008).
115. Zagrebelsky, M., Tacke, C. & Korte, M. BDNF signaling during the lifetime of dendritic spines. *Cell Tissue Res* **382**, 185–199 (2020).
116. Rajan, I. & Cline, H. T. Glutamate receptor activity is required for normal development of tectal cell dendrites in vivo. *J Neurosci* **18**, 7836–7846 (1998).
117. Alvarez, V. A., Ridenour, D. A. & Sabatini, B. L. Distinct structural and ionotropic roles of NMDA receptors in controlling spine and synapse stability. *J Neurosci* **27**, 7365–7376 (2007).
118. Spiga, S., Mulas, G., Piras, F. & Diana, M. The 'addicted' spine. *Front Neuroanat* **8**, 110 (2014).
119. Rasakham, K. *et al.* Synapse density and dendritic complexity are reduced in the prefrontal cortex following seven days of forced abstinence from cocaine self-administration. *PLoS One* **9**, e102524 (2014).
120. DePoy, L. M. & Gourley, S. L. Synaptic Cytoskeletal Plasticity in the Prefrontal Cortex Following Psychostimulant Exposure. *Traffic* **16**, 919–940 (2015).
121. Luppi, A. I. *et al.* Contributions of network structure, chemoarchitecture and diagnostic categories to transitions between cognitive topographies. *Nat. Biomed. Eng* **8**, 1142–1161 (2024).
122. Noonan, M. A., Choi, K. H., Self, D. W. & Eisch, A. J. Withdrawal from cocaine self-administration normalizes deficits in proliferation and enhances maturity of adult-generated hippocampal neurons. *J Neurosci* **28**, 2516–2526 (2008).
123. Crews, F. T. & Nixon, K. Mechanisms of neurodegeneration and regeneration in alcoholism. *Alcohol Alcohol* **44**, 115–127 (2009).
124. Larivière, S. *et al.* The ENIGMA Toolbox: multiscale neural contextualization of multisite neuroimaging datasets. *Nat Methods* **18**, 698–700 (2021).
125. Benjamini, Yoav & Hochberg, Yosef. Controlling the False Discovery Rate: A Practical and Powerful Approach to Multiple Testing. *Journal of the Royal Statistical Society* 289–300 (1995).
126. Rubinov, M. & Sporns, O. Complex network measures of brain connectivity: Uses and interpretations. *NeuroImage* **52**, 1059–1069 (2010).
127. Burt, J. B., Helmer, M., Shinn, M., Anticevic, A. & Murray, J. D. Generative modeling of brain maps with spatial autocorrelation. *Neuroimage* **220**, 117038 (2020).
128. van den Heuvel, M. P. & Sporns, O. An anatomical substrate for integration among functional networks in human cortex. *J Neurosci* **33**, 14489–14500 (2013).

a. Datasets

ENIGMA structural MRI dataset (n=2782, HC=1951)

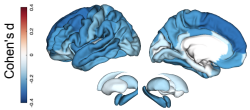

Case-control morphometric maps

Fig. 2, Tables S4–S5

HCP functional and diffusion MRI dataset (n=207)

FC

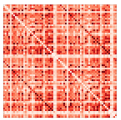

↓

Normative functional and structural connectome

SC

b. Network-based atrophy models

i) Hub vulnerability *Fig. 3, Tables S10–S13*

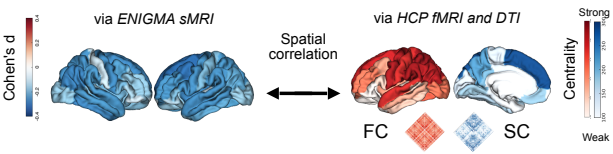

ii) Epicenter mapping *Fig. 4, Tables S14–S19*

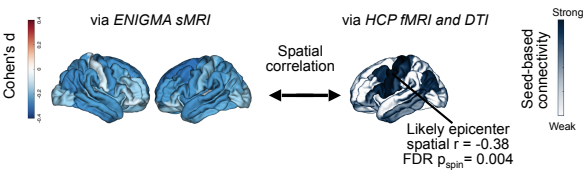

c. Robustness and generalizability

SUD-specific

Fig. 2e, Fig. 4c, Tables S4-S5, S14-S19

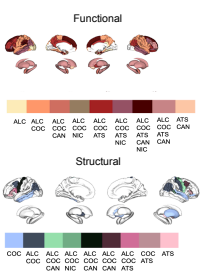

Age and sex effects

Fig. 2c,d, Fig. S4, Tables S20–24

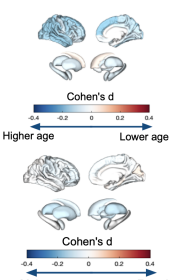

Subject-level analysis

Fig. S5, Table S25

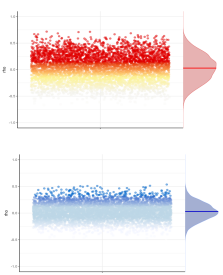

d. Cross-disorder comparison

Fig. 5, Tables S31–S38

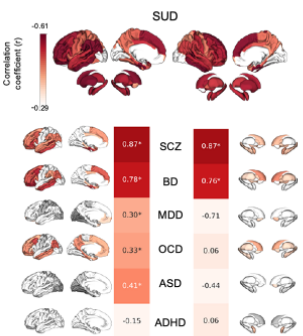

e. Neurotransmitter gradients

Fig. 6, Table S39

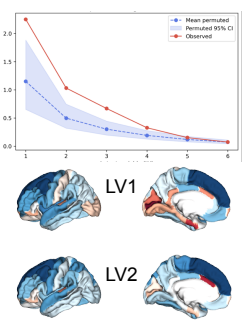

a. Demographics

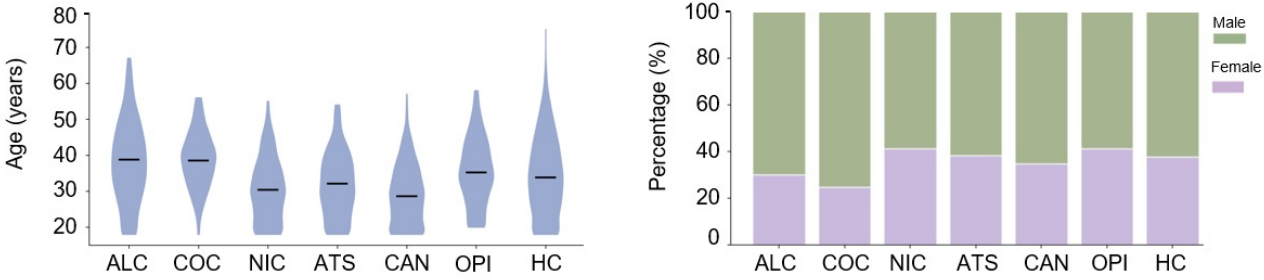

b. Morphometric differences across all SUD

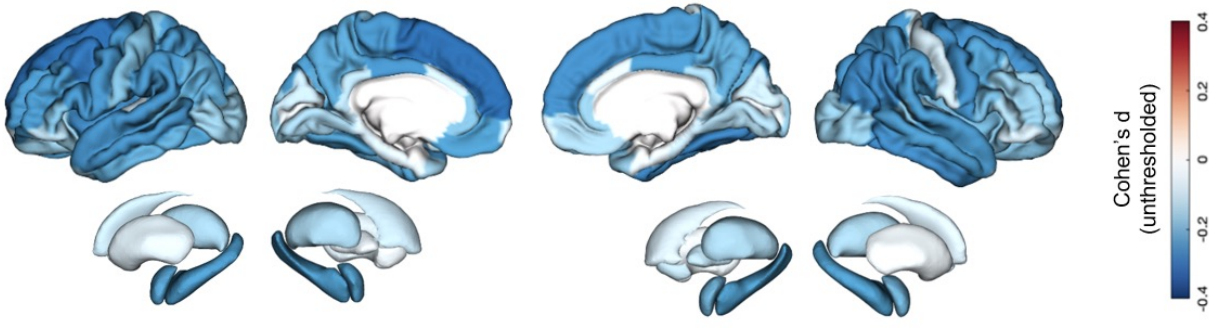

c. Age by SUD interaction effects

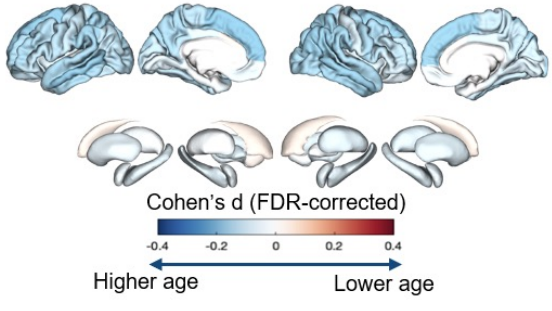

d. Sex by SUD interaction effects

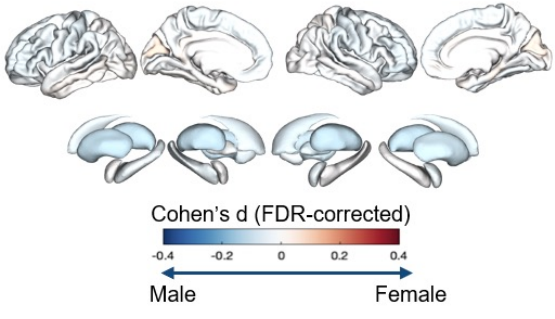

e. Morphometric differences of specific SUD

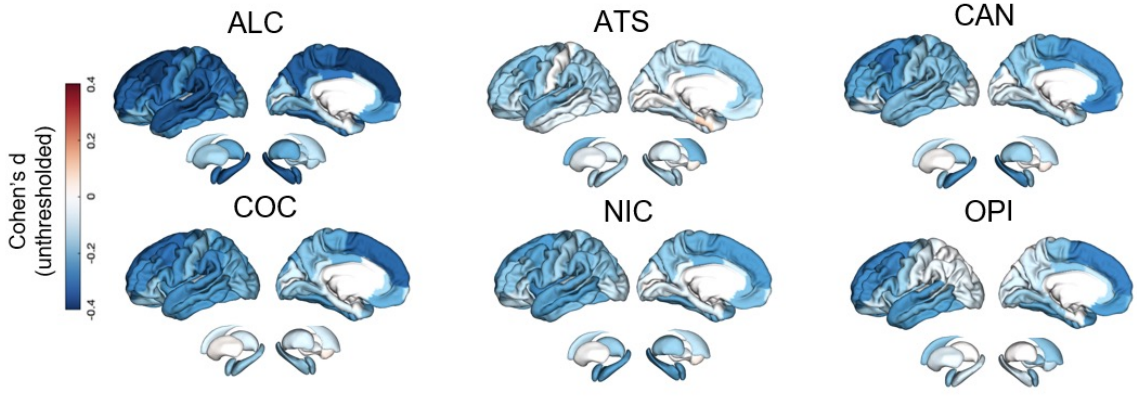

a. Hub vulnerability analysis

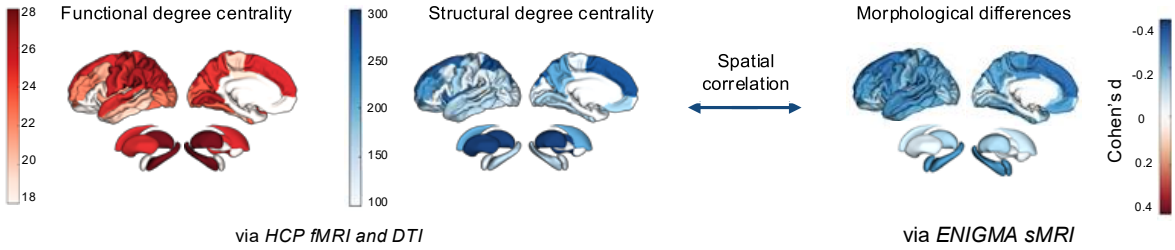

b. Cortical and subcortical hub vulnerability across all SUD

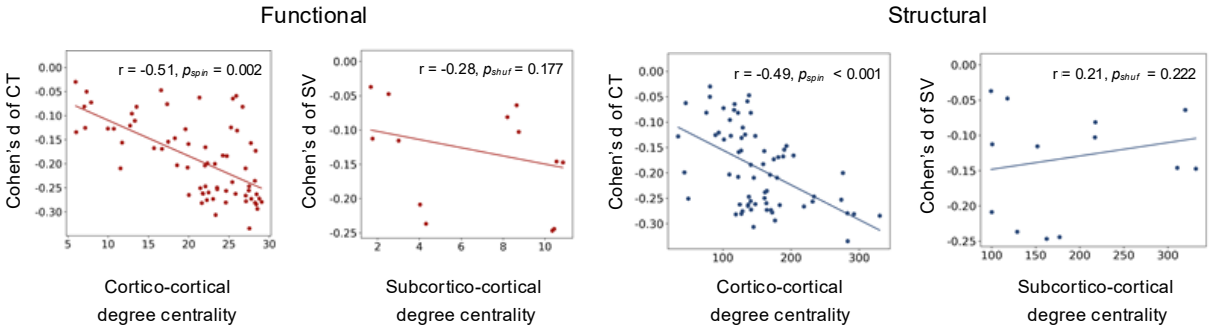

c. Cortical hub vulnerability in single SUD

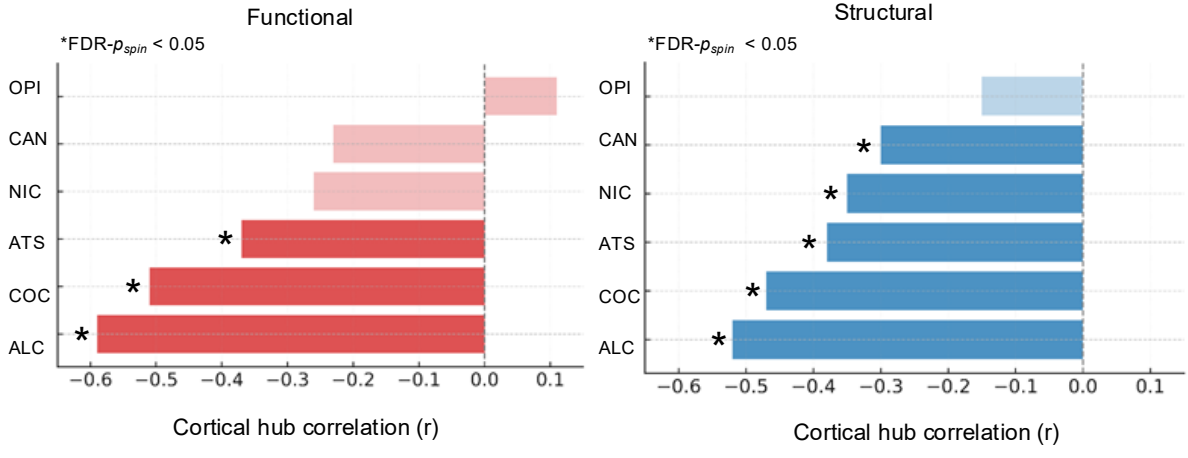

a. Network-based epicenter mapping model

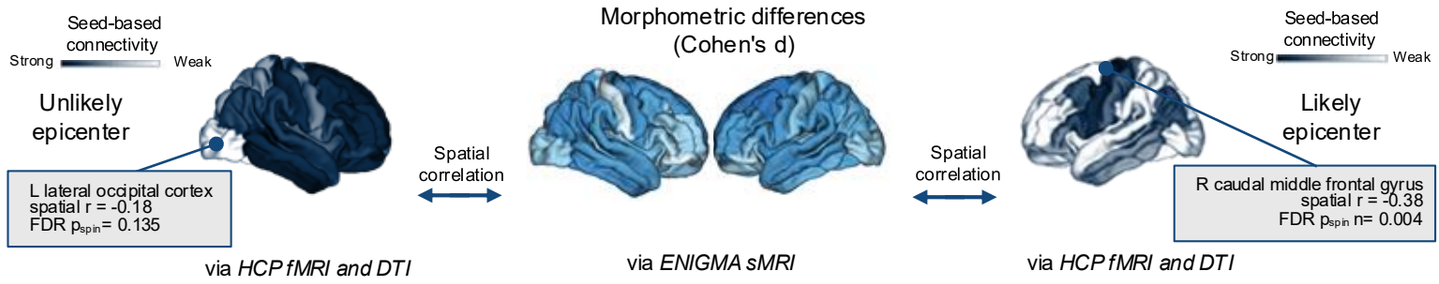

b. Cortical and subcortical epicenter maps of combined SUD

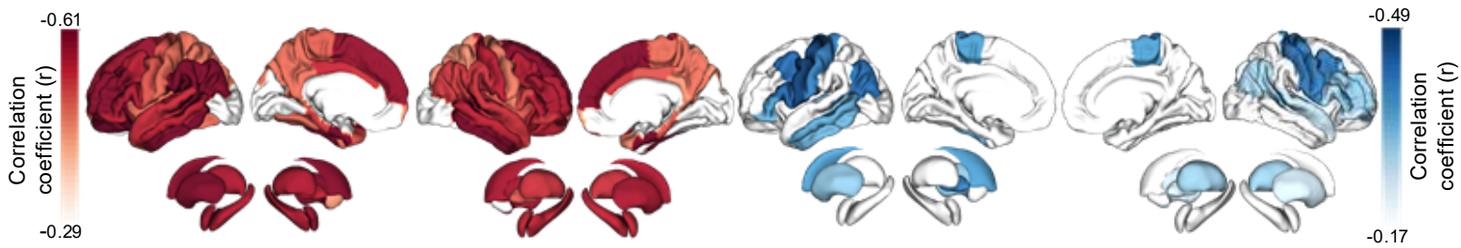

c. Unique and overlapping epicenters of Substance Use Disorders

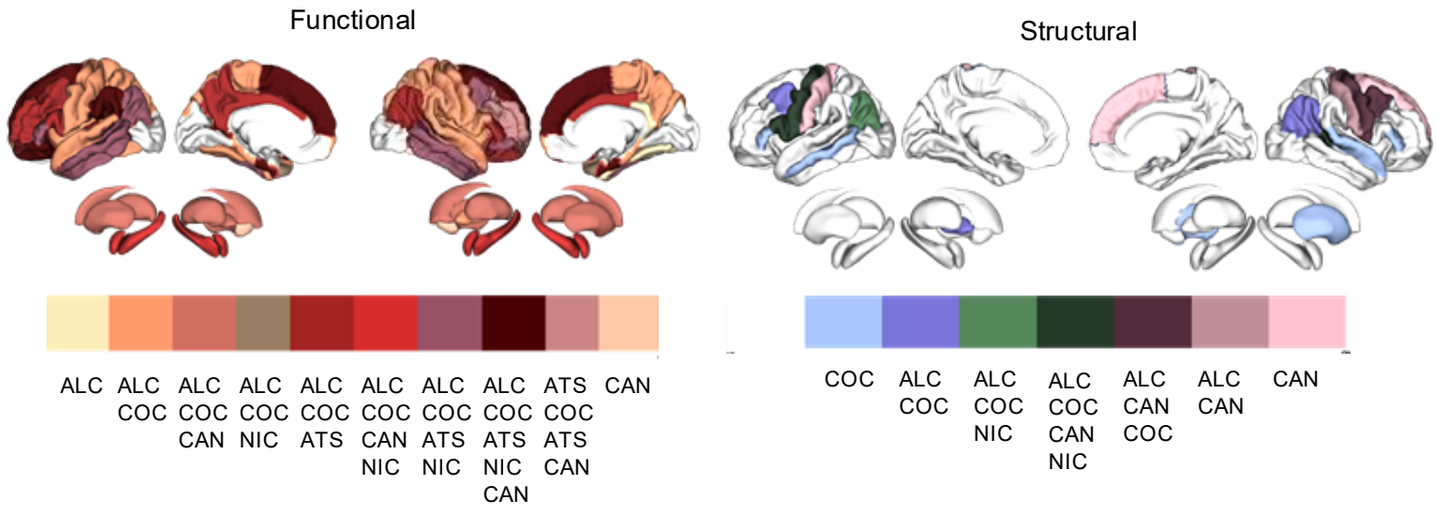

a. Transdiagnostic correlations of SUD epicenters

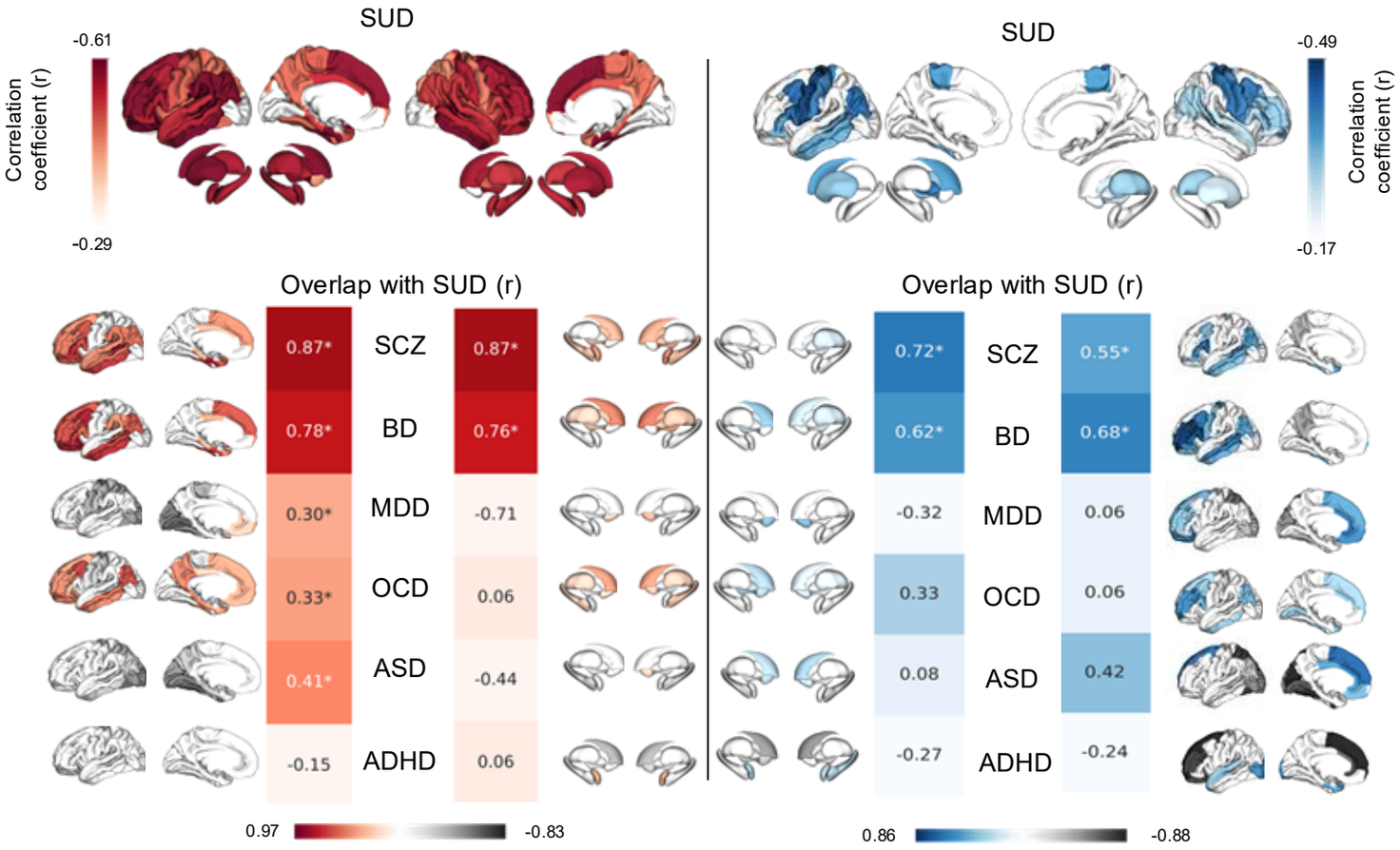

b. Transdiagnostically shared epicenters in SUD

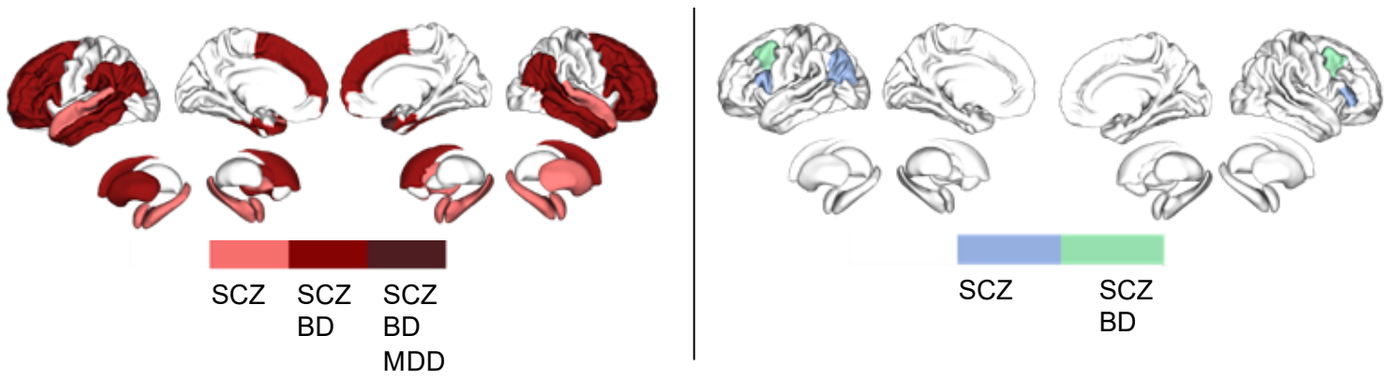

a. Permutation testing of significant LVs

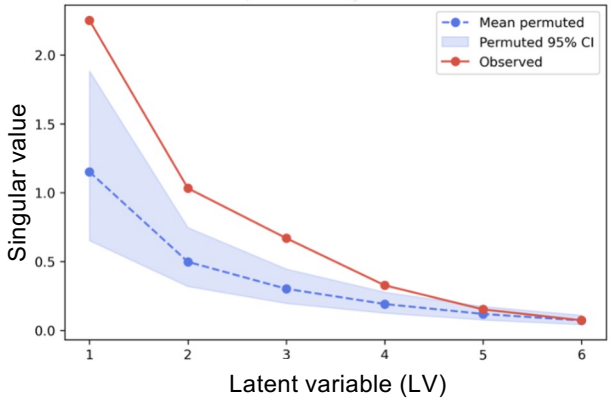

b. Percentage covariance explained

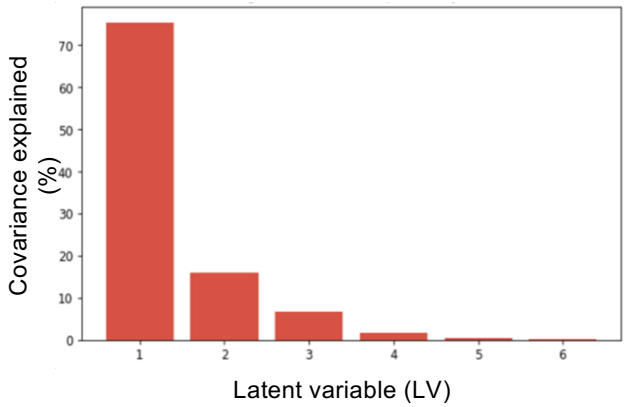

c. Projection of LV1-LV2 on brain surface

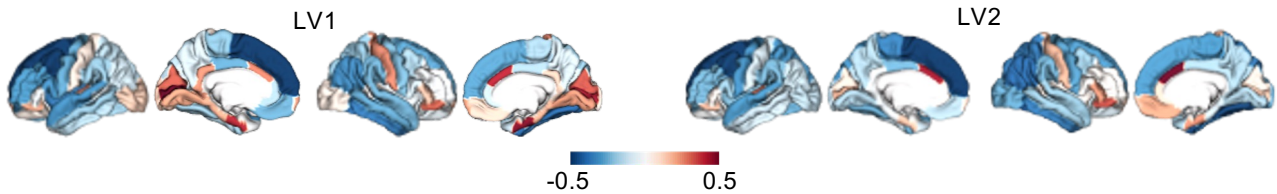

d. Loadings of LV1-LV2

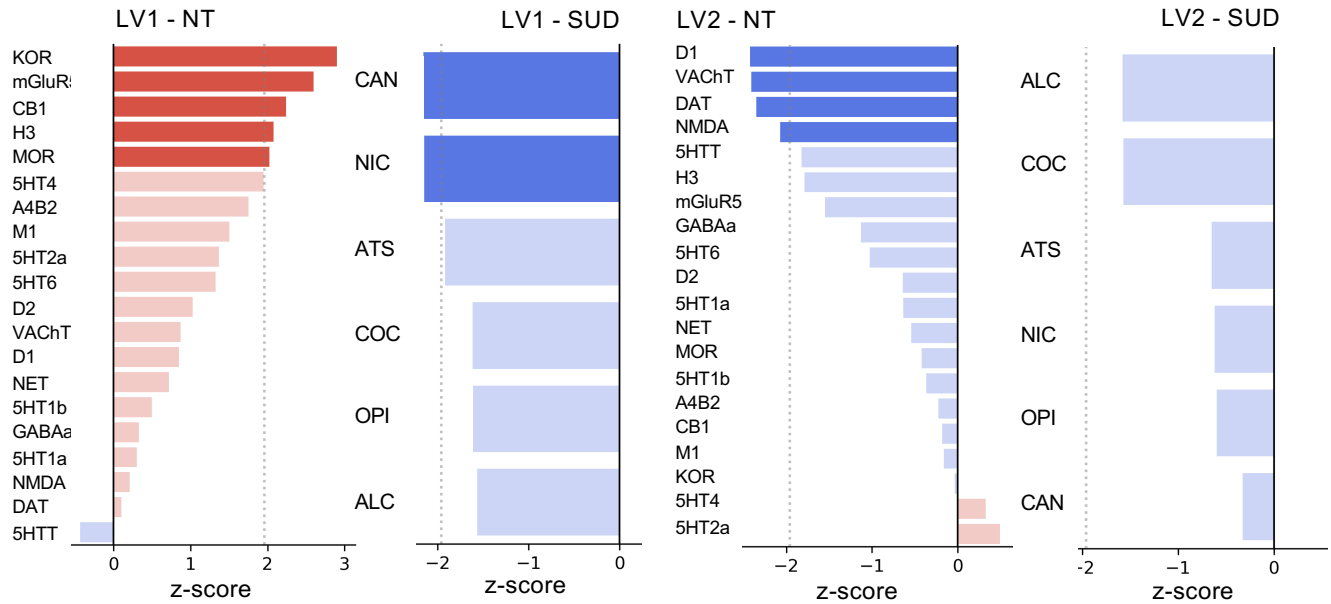
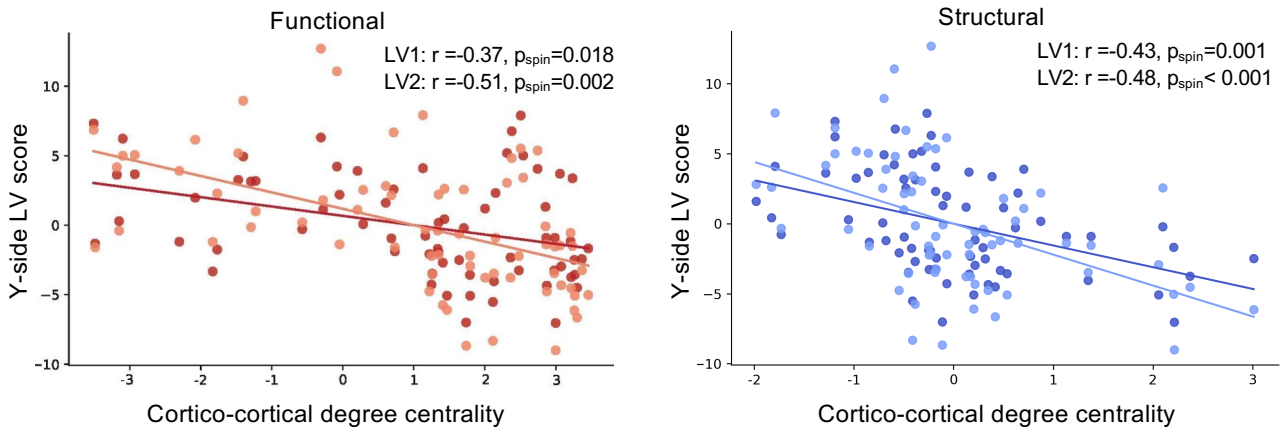
e. Hub vulnerability model for LV1-LV2